

# Geochemistry, Geophysics, Geosystems®



## RESEARCH ARTICLE

10.1029/2024GC011509

# Magma Differentiation, Contamination/Mixing and Eruption Modulated by Glacial Load—The Volcanic Complex of The Pleiades, Antarctica

Samuele Agostini<sup>1</sup> , Noemi Leone<sup>2</sup>, John L. Smellie<sup>3</sup> , and Sergio Rocchi<sup>2</sup> 

<sup>1</sup>Istituto di Geoscienze e Georisorse, Consiglio Nazionale delle Ricerche, Pisa, Italy, <sup>2</sup>Dipartimento di Scienze della Terra, Università di Pisa, Pisa, Italy, <sup>3</sup>Department of Geology, University of Leicester, Leicester, UK

### Key Points:

- The Pleiades complex (NVL, Antarctica) is made up of some 20 monogenetic cones aged 900–0 ka, defining a complete Na-alkaline trend
- Fractionation models show much larger volumes of primitive magmas, indicating the occurrence of an unusually large magma plumbing system
- A climax of activity occurred during the last glacial maximum (30 ka). Thickness variation of the ice cap may have influenced volcanic activity

### Correspondence to:

S. Agostini and S. Rocchi,  
s.agostini@igg.cnr.it;  
sergio.rocchi@unipi.it

### Citation:

Agostini, S., Leone, N., Smellie, J. L., & Rocchi, S. (2024). Magma differentiation, contamination/mixing and eruption modulated by glacial load—The volcanic complex of The Pleiades, Antarctica. *Geochemistry, Geophysics, Geosystems*, 25, e2024GC011509. <https://doi.org/10.1029/2024GC011509>

Received 15 FEB 2024

Accepted 1 MAY 2024

### Author Contributions:

**Conceptualization:** Samuele Agostini, Sergio Rocchi

**Data curation:** Samuele Agostini, Noemi Leone, John L. Smellie, Sergio Rocchi

**Formal analysis:** Samuele Agostini, Noemi Leone

**Funding acquisition:** Samuele Agostini, Sergio Rocchi

**Investigation:** Samuele Agostini, Noemi Leone, John L. Smellie, Sergio Rocchi

**Methodology:** Samuele Agostini

**Project administration:** Sergio Rocchi

© 2024 The Author(s). Geochemistry, Geophysics, Geosystems published by Wiley Periodicals LLC on behalf of American Geophysical Union.

This is an open access article under the terms of the [Creative Commons Attribution-NonCommercial-NoDerivs License](#), which permits use and distribution in any medium, provided the original work is properly cited, the use is non-commercial and no modifications or adaptations are made.

**Abstract** The Pleiades Volcanic Field is made up of some 20 monogenetic, partly overlapping scoria and spatter cones, erupted in the last 900 ka, cropping out from the ice close to the head of the Mariner Glacier in northern Victoria Land, Antarctica. Erupted products vary from hawaiite to trachyte, defining a complete mild Na-alkaline differentiation trend. Mafic samples are characterized by multi-elemental patterns typical of OIB magmas, moderately low  $^{87}\text{Sr}/^{86}\text{Sr}$  (0.7037) and high  $^{143}\text{Nd}/^{144}\text{Nd}$  (0.51284), with a clear within-plate affinity, indicating a subcontinental lithospheric source. With increasing  $\text{SiO}_2$ ,  $^{87}\text{Sr}/^{86}\text{Sr}$  ratios increase up to 0.7052 and  $^{143}\text{Nd}/^{144}\text{Nd}$  decrease to 0.51277, supporting the hypothesis of open-system evolution, with significant crustal assimilation during fractional crystallization. The erupted volume of most evolved products ( $\sim 7 \text{ km}^3$ ), according to fractionation models, suggests that primitive magmas should have been more than 10 times larger, indicating the occurrence of a large magma plumbing system, unexpected for a volcanic field of monogenetic scoria cones. The occurrence of a complete fractionation trend with large magma chambers and large assimilation rate is unusual, if not unique, among the alkali basaltic volcanic fields and it is matched by a climax of activity during the last glacial maximum (30 ka), as indicated by new  $^{40}\text{Ar}$ - $^{39}\text{Ar}$  ages ( $30 \pm 3 \text{ ka}$  and  $25 \pm 2 \text{ ka}$ ) for samples from the two most prominent edifices. Therefore, we hypothesize a role of a thick ice cap in suppressing eruptions and ultimately leading to prolonged magma residence time in the subsurface, favoring significant fractionation coupled with unusual high rates of crustal assimilation.

**Plain Language Summary** The Pleiades volcanic field is made up of some 20 monogenetic scoria and spatter cones, which erupted in the last 900 ka close to the head of the Mariner Glacier in northern Victoria Land, Antarctica. The erupted products are very unusual for alkali basaltic volcanism: indeed, whereas few samples show clear within-plate subcontinental lithospheric characteristics and were directly derived from the mantle source, most of the products formed after extensive fractional crystallization matched by significant crustal assimilation, implying that primitive magma volumes are 10 times larger than outcropping products in an unusually large magma plumbing system. These peculiar features coincided with a climax of activity during the last glacial maximum (30–25 ka). Therefore, we speculate that a thick ice cap favored high rates of crystal fractionation coupled with crustal assimilation and was responsible for increasing magma residence times in chambers at crustal depths and suppressing the eruptive potential of magmas.

## 1. Introduction

The timing of volcanic eruptions in glaciated terrains is potentially modulated by climate-controlled variations in the glacio-lithostatic load, that modify the failure conditions around magma chambers as well as the pressure acting on underlying volcanic plumbing systems (Glazner et al., 1999; Grove, 1974; Huybers & Langmuir, 2009; MacLennan et al., 2002; Rawson et al., 2016; Sigmundsson et al., 2010; Sigvaldason et al., 1992; Smellie & Edwards, 2016). Even relatively small fluctuations in ice thickness can affect the stability of very shallow crustal chambers, delaying or precipitating eruptions. In detail, at a depth where the stress state changes from tensile to compressive, magmas rising along fractures will likely pond, forming shallow sill-like magma reservoirs (Geyer & Bindeman, 2011; Wilson & Russell, 2020). It is therefore likely that rising magmas will experience extended residence times in the crust during glacial periods, which would allow them to crystallize and differentiate over longer times to a greater extent at higher pressure. The prolonged crystallization of nominally anhydrous minerals in ponding magmas also increases the concentration of volatiles in the melt. Eventually, during glacial retreat, the restoration of a tensional stress regime in the shallow crust is likely to initiate

**Resources:** Samuele Agostini, Sergio Rocchi  
**Supervision:** Samuele Agostini, John L. Smellie, Sergio Rocchi  
**Validation:** Samuele Agostini  
**Visualization:** Samuele Agostini, Sergio Rocchi  
**Writing – original draft:** Samuele Agostini, Noemi Leone, Sergio Rocchi  
**Writing – review & editing:** Samuele Agostini, John L. Smellie, Sergio Rocchi

vesiculation, triggering eruptions of magmas characterized by high ratios of most incompatible to least incompatible elements (Nyland et al., 2013). Moreover, models of glacial retreat in Iceland have shown that additional magma can be generated in the mantle by glacial unloading (Jull & McKenzie, 1996; Pagli & Sigmundsson, 2008; Sigmundsson et al., 2010; Slater et al., 1998).

However, how these effects will influence the eruption likelihood at subglacial volcanoes and therefore the length of time that magma is stored in shallow chambers has been addressed in a few cases in the northern hemisphere (Edwards et al., 2002; Geyer & Bindeman, 2011; Glazner et al., 1999; MacLennan et al., 2002), while investigations for southern hemisphere volcanoes are lacking.

In Antarctica, volcanic activity has occurred since the Miocene in several glaciated regions (LeMasurier & Thomson, 1990; Smellie et al., 2021a, 2021b). In northern Victoria Land (NVL), volcanism generated an inland scattered group of stratovolcanoes and monogenetic scoria cones located on the thick cratonic lithosphere, and a coastal belt of voluminous fissure-fed shield volcanoes sitting on the most attenuated (necked?) lithosphere, marking the transition to the continental crust of the Ross Sea, attenuated during Cenozoic rifting processes (Panter et al., 2018; S. Rocchi & Smellie, 2021; S. Rocchi et al., 2005; Smellie & Rocchi, 2021). Among the inland group of northern Victoria Land volcanoes, the Quaternary Pleiades Volcanic Field has been selected for this work owing to the occurrence of a continuous compositional evolutionary lineage (Kim et al., 2019). It has been therefore possible to address the issue of temporal variations in the composition of the erupted magmas in relation to changes in thickness and extent of the ice cover.

## 2. The Pleiades Volcanic Field

The Cenozoic evolution of the West Antarctic Rift System is linked to igneous activity starting in the Eocene (LeMasurier & Thomson, 1990; S. Rocchi & Smellie, 2021; S. Rocchi et al., 2002). In the western Ross Embayment, Antarctica (Figure 1) volcanic products collectively belong to the McMurdo Volcanic Group (MMVG; Kyle, 1990a; LeMasurier & Thomson, 1990; Smellie et al., 2021a, 2021b) and record eruptions in a variably glaciated environment from the Miocene to the Present (Smellie, Rocchi, & Armienti, 2011; Smellie, Rocchi, Gemelli, et al., 2011; Smellie et al., 2014, 2018). The volcanic rocks of northern Victoria Land are grouped into (a) the Hallett Volcanic Province, including Adare Peninsula, Hallett Peninsula, Daniell Peninsula and Coulman Island, which comprise composite, elongated (c. 25 × 40–75 km) dominantly shield volcanoes erupted from fissures, and (b) the Melbourne Volcanic Province, including Mount Melbourne (c. 25 × 55 km) and Mount Overlord stratovolcanoes, as well as The Pleiades, and Malta Plateau (c. 30 × 50 km) volcanic fields (Smellie & Rocchi, 2021). Additionally, numerous small scattered volcanic centers, mainly scoria cones, are present inland between Mount Melbourne and Adare Peninsula (Northern Local Suite). The volcanic products are dominated by lavas, breccia and scoria deposits, according to the eruption style (Smellie & Rocchi, 2021; Smellie, Rocchi, & Armienti, 2011). Compositionally, they correspond to a moderately alkaline sodic association that is essentially bimodal: basaltic products are dominant (Hamilton, 1972), mostly basanites and alkali basalts-hawaiites, along with rare nephelinites; evolved products are mainly trachytes and minor rhyolites, some of which are peralkaline. Most mafic samples (Nardini et al., 2009) were extruded as small lava flows, commonly marking the end of explosive activity in monogenetic scoria cones. Products of intermediate composition, such as mugearites and benmoreites, are volumetrically minor. Strongly alkaline compositions are typically very uncommon in northern Victoria Land, and they are limited to phonolites and rare tephrites and foidites.

The Pleiades Volcanic Field is an isolated cluster of volcanic outcrops (Figure 1) surrounded by snow and ice at the edge of the polar plateau overlooking the head of the Mariner Glacier, at a general elevation of c. 2,500 m above sea level (asl). At c. 120 km from the Ross Sea coast, it is the furthest inland outcrop of the Melbourne Volcanic Province (Esser & Kyle, 2002; Kyle, 1982, 1990c). From a volcanological point of view, the Pleiades are a group of at least 20 small sometimes nested scoria cones with prominent well-preserved craters and two domes (Mt. Taygete and an unnamed feature, C11, Kyle, 1982) that extend c. 16 km in a northeasterly direction (Figure 1). Only four centers have a geographic name (i.e., Taygete, Alcyone, Pleiones and Atlas), others were numbered C1–C12 (after Kyle (1982)), and at least six additional cones can now be recognized (here labeled C5A, C5B, C6A, C7A, C11A, and C11B, Figure 1a and data repository 1). The slightly arcuate distribution of cones led Kyle (1990c) to infer that the centers were distributed around a caldera rim. The highest points are Mount Atlas (c. 3,040 m) and Mount Pleiones (c. 3,020 m), rising c. 500 m above the surrounding Evans N ev  snowfield, and

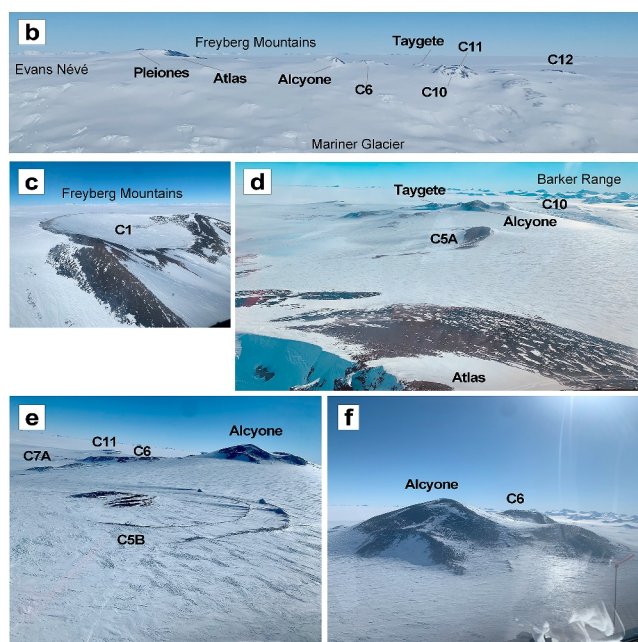
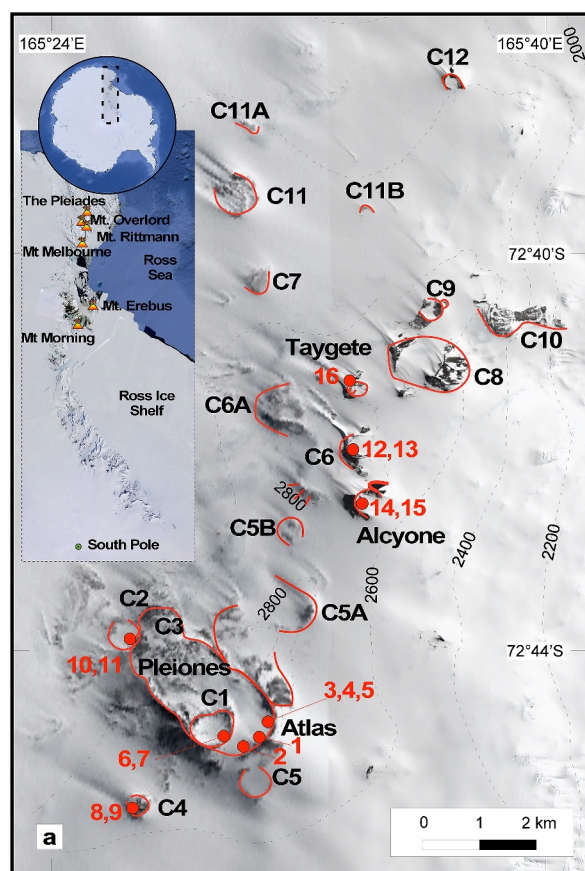


Figure 1.

regarded as part of a small composite volcano comprising several overlapping and nested scoria cones (Esser & Kyle, 2002). The Mount Atlas–Mount Pleiones center consists of five nested craters c. 500–1,000 m in diameter, formed of scoria and numerous large dense bombs, and at least two smaller flank scoria cones on the south side. Although the three main craters were described as formed by oxidized scoriaceous lavas (Kyle, 1982; Nathan & Schulte, 1968), like most of the other nunataks, they are pyroclastic.

Most of the other outcrops to the NE are also pyroclastic cones very similar to the Mount Atlas–Mount Pleiones cluster and have a variety of mafic compositions. By contrast, Taygete Cone is a pale-colored trachyte dome. The low-lying outcrop c. 4 km to the NW of Taygete Cone (C11 outcrop) (Kyle, 1982) may also be a dome made of evolved products mantled by mafic lava. Finally, trachyte pumice lapilli are common on several nunataks (Kyle, 1982; Nathan & Schulte, 1968). They also occur as abundant large broken bombs on the small nunatak c. 1,200 m north of Alcyone Cone (outcrop C6 of Kyle (1982)), suggesting closeness to the vent (Smellie & Rocchi, 2021).

The compositional variability of the volcanic rocks is broad, with most rocks defining a continuous, silica-saturated to slightly undersaturated lineage from alkali-basalt to trachyte. The additional occurrence of undersaturated mafic-intermediate samples evolving from alkali basalt-basanite to tephriphonolite compositions led to the suggestion that there are two main evolutionary lineages (Kim et al., 2019; Kyle & Rankin, 1976).

The Pleiades are regarded as very young or even dormant based on the undissected appearance of the cones (Kyle, 1990c; Nathan & Schulte, 1968; Riddolls & Hancox, 1968) and initial K-Ar geochronological data (Armstrong, 1978). More recent  $^{40}\text{Ar}$ – $^{39}\text{Ar}$  isotopic ages (Esser & Kyle, 2002) range from  $847 \pm 12$  to  $6 \pm 6$  ka, with the latter determined for the Taygete dome potentially confirming the dormant nature of the volcanic complex. However, evidence for hydrothermal alteration at the Taygete Cone (Esser & Kyle, 2002; Kyle, 1982) suggests that the youngest age may be unreliable (Smellie & Rocchi, 2021). The potential very young age of evolved products at The Pleiades has led to the suggestion that the 1254 CE and other recent tephra recovered from the Talos Dome ice core could have possibly originated from there (Narcisi et al., 2001, 2017). However, further investigations on marine and ice cores have demonstrated that these “historical” eruptions were sourced from Mount Rittmann volcano in northern Victoria Land (Di Roberto et al., 2019; Lee et al., 2019). In summary, four main periods of activity can be recognized based on the published  $^{40}\text{Ar}$ – $^{39}\text{Ar}$  isotopic ages. The oldest phase was active in the central-northern part of the volcanic field (north of Alcyone Cone and east of Taygete Cone) at c. 850–820 ka. Two intermediate phases then occurred at  $\sim 630$  ka and between c. 340 and 310 Ma in the two northernmost outcrops. Finally, after a lull of c. 200 ka, activity resumed at  $93 \pm 4$  ka at the north-easternmost end of the field prior to migrating to the southern end of The Pleiades (Mount Atlas–Pleiones-

**Figure 1.** (a) Location and Map of The Pleiades Volcanic Field, NVL, Antarctica. Isohyps from 1:250,000 Topographic Map of Antarctica, USGS, Freyberg Mountains Sheet; Sat view from Google Earth. Cone numbering modified after Kyle (1982) (b–f) Field view of The Pleiades Volcanic Field: (b)—Aerial view of The Pleiades volcanic field from East; (c) C1 scoria cone from the top of Mt. Atlas; (d) Mt. Taygete and Mt. Alcyone from the top of Mt. Atlas; (e, f) Alcyone dome and other surrounding centers.

Alcyone), with eruptions between c. 70 and 20 ka for emplacement of the Taygete dome, followed by a very young outlier event occurring at not well constrained age of  $6 \pm 6$  ka.

### 3. Samples and Methods

The volcanic edifices of The Pleiades have been the subject of several investigations between 1982 (Kyle, 1982) and 2019 (Kim et al., 2019). For this study, in the frame of the 30th Italian Antarctic Expedition, we collected 16 samples from seven different cones (Figure 1, data repository 2). Samples comprise lavas, bombs, scoriae and pumices, selected to be representative of the range of volcanological, petrographic and geochemical variations present. For these 16 samples, here we present a complete data set including petrographic features, major and trace element compositions, and Sr-Nd-Pb radiogenic isotope data. Our data are presented along with literature data (Esser & Kyle, 2002; Kim et al., 2019; Kyle, 1986). The complete data set is presented in data repository 3.

Whole-rock major and trace element analyses were measured by XRF (X-Ray Fluorescence) and ICP-MS (Inductively Coupled Plasma-Mass Spectrometry), respectively, at the Dipartimento di Scienze della Terra, University of Pisa.

Radiogenic (Sr-Nd-Pb) isotopic analyses and  $^{40}\text{Ar}$ - $^{39}\text{Ar}$  age determinations were carried out at the Istituto di Geoscienze e Georisorse—CNR of Pisa (Italy). For isotope analysis, rock powders were dissolved in  $\text{HF} + \text{HNO}_3$ . Sr, Nd and Pb were separated chromatographically and measured via TIMS (Thermal Ionization Mass Spectrometry) with a Finnigan Mat 262. Age determinations were performed by the  $^{40}\text{Ar}$ - $^{39}\text{Ar}$  method on alkali feldspar separates on two selected samples, JS3 pumice from Mount Atlas cone and JS16 lava dome from Taygete cone (data repository 4). Experimental techniques followed those previously described in Di Vincenzo et al. (2010).

A full and detailed description of the analytical methods is available in the Data Repository.

## 4. Results

### 4.1. Petrographic Features

Rocks from The Pleiades vary both in the types of products as well as chemical composition. They appear macroscopically as gray or dark gray lava, black scoriae and bombs, and light gray pumices. As a whole, petrographic textures exhibit large variability: pumices and scoriae are highly vesiculated, glassy and aphyric, whereas lavas are usually subaphyric or porphyritic. In Figure 2 some microscopy images are presented, more pictures are available in Data Repository Figures 1 and 2).

Relevant petrographic features are the occurrence of abundant olivine in the most mafic and intermediate compositions (Figures 2a and 2b) both as phenocrysts and in the groundmass. Hawaiites and benmoreites are also characterized by abundant phenocrysts of clinopyroxene and Ca-rich plagioclase along with minor olivine (Figures 2a and 2b), and amphibole in a few samples (Figures 2c and 2d). Alkali feldspars are found as microlites in mafic-intermediate lavas, and as phenocrysts in the most evolved samples (Figures 2e–2h). Groundmasses are usually hypocristalline, with variable numbers of the same phases observed as phenocrysts along with anorthoclase and Fe-Ti oxides.

The most evolved samples have both Na-rich plagioclase and anorthoclase/sanidine as the largest and most abundant phenocrysts (Figure 2), along with clinopyroxene  $\pm$  amphibole  $\pm$  biotite, with smaller Fe-rich olivine and opaques confined to the groundmass. Some trachytes exhibit pilotaxitic textures (Figure 2), and sometimes antirapakivi structures are observed (e.g., sample JS 12; Figures 2e and 2f). Notably, no quartz is present even in the most evolved products, which may exhibit a few percent of normative Qtz in the CIPW norm (e.g. JS16, Data Repository Table 3). By contrast, feldspathoids are extremely rare and occur as microlites in a few of the normative samples.

### 4.2. Major and Trace Elements

The composition of the collected samples varies with remarkable continuity and there are no compositional gaps in the Total Alkalis versus  $\text{SiO}_2$  diagram (TAS; Figure 3a) defining a continuous silica-undersaturated (1–5.7 of normative *ne*) to silica-saturated (*ol-hy*-normative with 1.3–4.5 of normative *hy*) trend, with most samples falling in the fields of basalts, trachybasalts, trachybasaltic andesites, trachyandesites and trachytes. Only a few of the

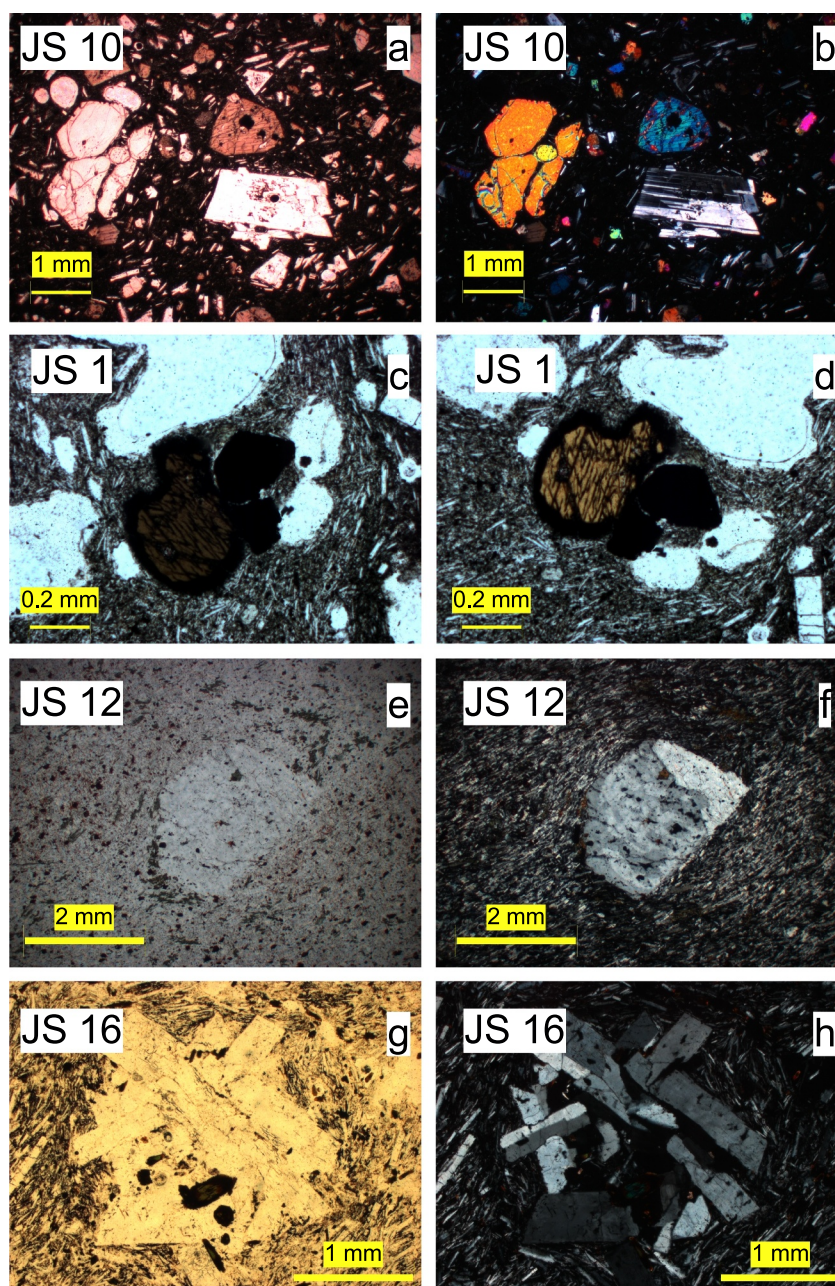


**Figure 2.** Petrography of The Pleiades samples—(a, b) Hawaiiite JS 10 (PPL and XPL) with ol, pl, and cpx phenocrysts in a hypocrySTALLINE aphanitic groundmass; (c, d) pleochroic microphenocryst of amphibole (PPL, PPL rotated of 90°) in a vesiculated pilotaxitic groundmass in benmoreite JS1; (e, f) antirapakivi texture in trachyte JS12 (PPL and XPL); (g, h) glomerophyres of alkali feldspar and plagioclase in a pilotaxitic groundmass in trachyte JS16 (PPL and XPL). More pictures and high-resolution images are available in the data repository Figures 1 and 2.

most evolved trachytic samples show very modest degrees of  $\text{SiO}_2$ -oversaturation (normative  $Q < 0.5$ ). When considering all available data from literature, it is of note that some scattered samples fall in the strongly undersaturated fields of TAS (basanites/tephrites, phonotephrites, and tephriphonolites) without defining a clear and continuous trend. The occurrence of these samples induced previous authors (Kyle, 1986) to call for the occurrence of two distinct trends at The Pleiades, called “strongly undersaturated sodic lineage” and “saturated to slightly undersaturated potassic lineage,” respectively. More recently, the main difference between these trends has been linked to the occurrence of abundant kaersutite in the undersaturated trend, and the occurrence of olivine and lack of kaersutite in the saturated trend (Kim et al., 2019). However, we observed widespread occurrence of

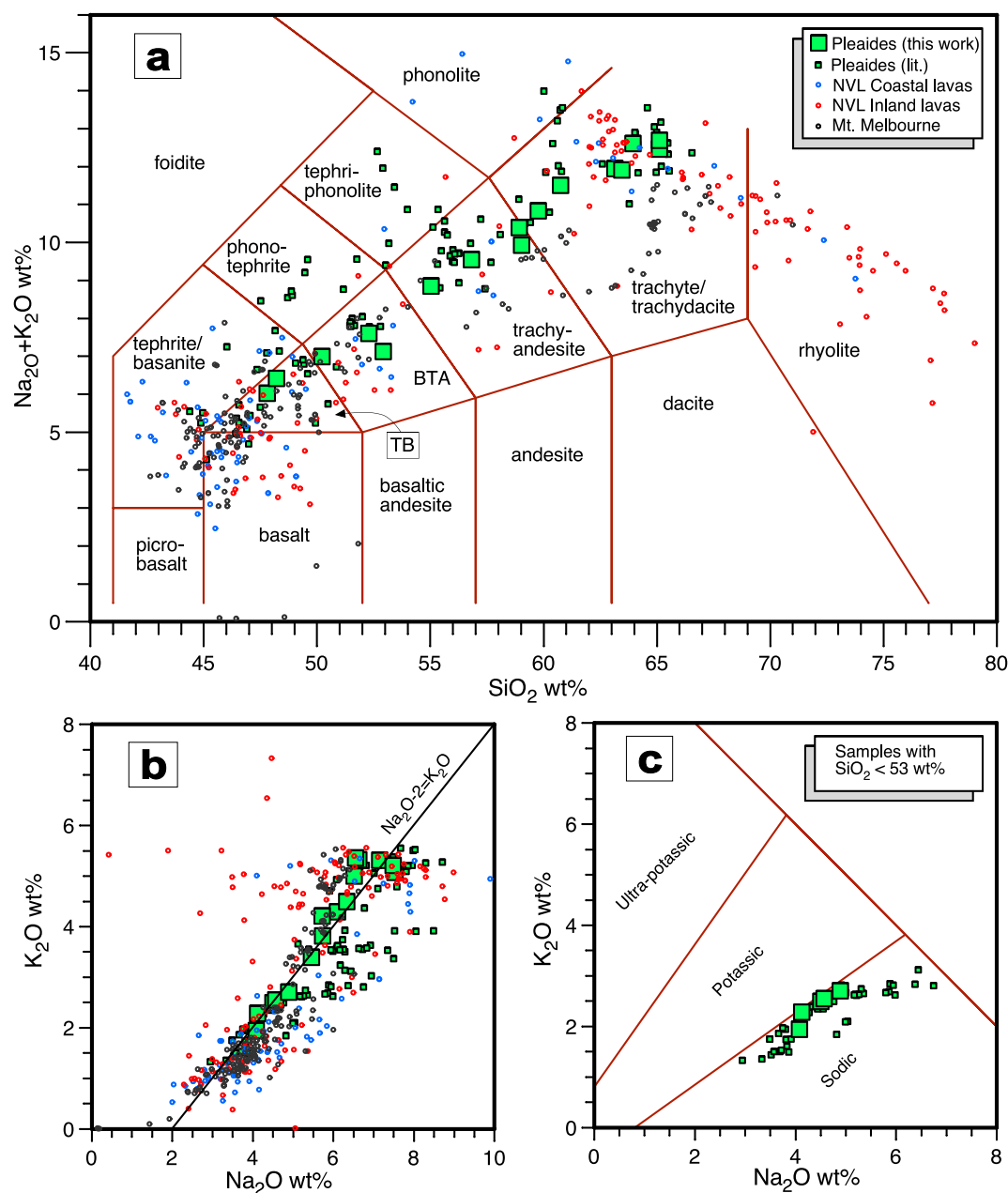


**Figure 3.** Total alkali versus Silica (a), K<sub>2</sub>O versus Na<sub>2</sub>O (b) and (c) classification diagrams for samples of The Pleiades Volcanic Field. Other volcanic rocks from the NVL region are plotted for comparative purposes (literature data sources in S. Rocchi and Smellie (2021) and references therein). Fields in (c) after Middlemost (1975).

amphibole phenocrysts, albeit in a minor amount, in samples belonging to the saturated-slightly undersaturated trend as well (e.g., Figures 2c and 2d, and data repository Figures 1 and 2).

Regarding the two putative lineages, it is notable that most samples from The Pleiades, both saturated and undersaturated, are actually Na-alkaline, having  $\text{Na}_2\text{O} - 2 > \text{K}_2\text{O}$  (Figure 3b), and the remaining samples have  $1 < \text{Na}_2\text{O} - \text{K}_2\text{O} < 2$ , thus approaching a Na- rather than a K-alkaline series. Hence, the whole of The Pleiades samples, regardless of their degree of saturation, exhibit a sodic affinity, and we suggest that a potassic lineage is not actually present in The Pleiades Volcanic Field.

This is even more evident when less evolved samples (i.e., those with SiO<sub>2</sub> < 53 wt%) are plotted on a K<sub>2</sub>O versus Na<sub>2</sub>O classification diagram (Figure 3c) on which all of them classify as sodic and define a single lineage. The

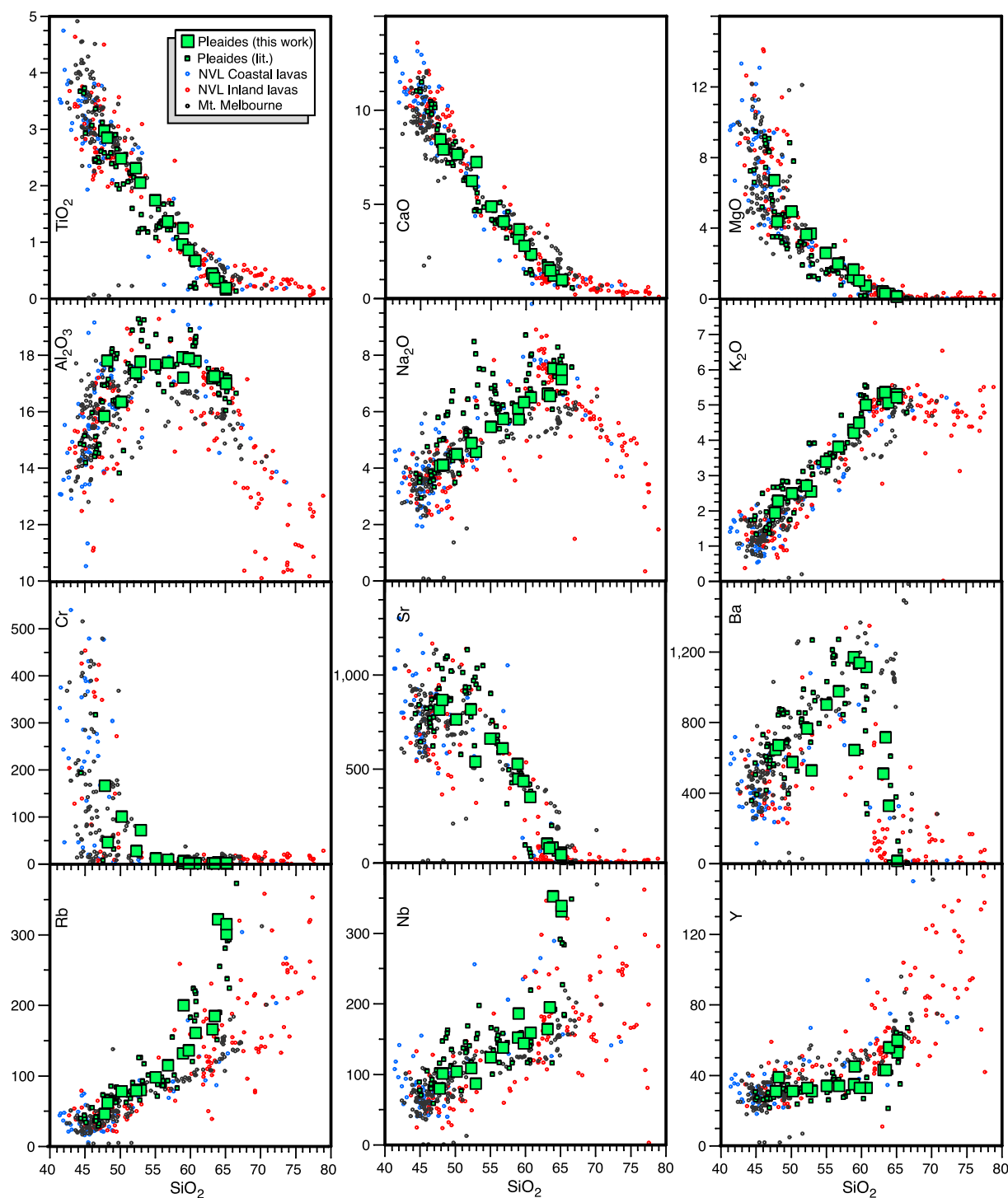


**Figure 4.** Selected major and trace element variations against  $\text{SiO}_2$  for samples of The Pleiades Volcanic Fields. Other volcanic rocks from the NVL region are plotted for comparative purposes (data sources as in Figure 3). More diagrams available in Data Repository Figures 3–5.

mild potassic affinity is restricted to a few of the more evolved rocks, and was acquired during magma differentiation, likely after removal of high Na/K phases, namely plagioclase.

Variation diagrams of selected major and trace elements of samples from The Pleiades are presented in Figure 4. More diagrams can be found in Data Repository Figures 3–5. The samples are compared with the three main

compositional/geographic groups of NVL lavas, that is, (a) the coastal lava from the shield volcanoes of Adare, Hallett and Daniell peninsulas and Coulman Island; (b) the inland lava from the Malta Plateau, Mount Rittmann, and isolated scoria cones of the Northern Local Suite; and (c) the central edifice of Mount Melbourne and its parasitic cones and satellite volcanoes.

As a whole, variations depicted by samples of The Pleiades are quite similar to volcanic products from northern Victoria Land belonging to the MMVG only when products with  $\text{SiO}_2$  wt% < 65 are considered. Indeed, many NVL lavas evolve up to c. 77 wt%  $\text{SiO}_2$ , whereas the most evolved samples from The Pleiades have  $\text{SiO}_2$  wt% < 65. As a consequence,  $\text{TiO}_2$ ,  $\text{CaO}$  and  $\text{P}_2\text{O}_5$  exhibit a linear negative trend for The Pleiades samples, whereas other inland lavas have evolved on a trend which is flattening at the most evolution stages;  $\text{MgO}$  is characterized by a downward-convex trend, with  $\text{MgO}$  contents in all the NVL samples approaching zero at  $\text{SiO}_2 \approx 62$  wt%;  $\text{FeO}^*$  (i.e., all iron calculated as  $\text{FeO}$ ) decreases linearly, down to values as low as 3 wt% for The Pleiades samples and is <1% in some of most evolved surrounding lava. The trend depicted by  $\text{Al}_2\text{O}_3$  is typically humped (i.e., convex-upward), being positive up to  $\text{SiO}_2 \approx 55$  wt%, then flattens for  $\text{SiO}_2 \approx 55$ –60 wt%, and finally tends to decrease with increasing  $\text{SiO}_2$ . The Pleiades samples exhibit well-defined major oxide trends, whereas the trends for other NVL lavas are more scattered. However, some dispersion, especially involving  $\text{Al}_2\text{O}_3$  enrichment, is also observed in some of the published samples of The Pleiades. Well-defined linear positive trends are also observed for our samples when alkalis ( $\text{Na}_2\text{O}$  and  $\text{K}_2\text{O}$ ) are plotted against  $\text{SiO}_2$ ; again, when considering other NVL samples, switches from positive to negative slopes and from positive to an almost flat trend is observed for  $\text{Na}_2\text{O}$  and  $\text{K}_2\text{O}$ , respectively, which is a phenomenon not recorded by The Pleiades samples since they lack compositions exceeding 65 wt%  $\text{SiO}_2$ . As for  $\text{Al}_2\text{O}_3$ , other NVL sample compositions are dispersed around the linear trends depicted by The Pleiades samples. They frequently show anomalous strong enrichment of  $\text{Na}_2\text{O}$  and, to a lesser extent  $\text{K}_2\text{O}$ , at comparable  $\text{SiO}_2$  contents.

Variation diagrams for compatible trace elements like Ni, Cr, V, and Co in The Pleiades samples exhibit a marked decrease with respect to  $\text{SiO}_2$  and tend to flatten close to zero at  $\text{SiO}_2 \approx 60$ –65 wt% except for Co. A remarkable difference between The Pleiades and other NVL lavas is observed for these elements in the more mafic samples: maximum values reached by The Pleiades lavas are notably lower than other NVL suites (e.g.,  $\approx 400$  vs.  $\approx 100$   $\mu\text{g/g}$  for Ni,  $\approx 500$  vs. 150  $\mu\text{g/g}$  for Cr). Notably also, Sr in The Pleiades lava behaves as a compatible element depicting an almost linear negative trend when plotted against  $\text{SiO}_2$ , whereas other NVL lavas have a more complex trend, being scattered and roughly positive for more mafic samples and flattened close to zero in more evolved compositions.

Most of the incompatible trace elements are characterized by positive trends apart from Ba, which tends to increase with  $\text{SiO}_2$  up to  $\approx 60$  wt% and then decreases very steeply. Most of the other incompatible elements, both Large Ion Lithophile Elements (LILE, such as Rb) and High Field Strength Elements (HFSE, such as Nb, Ta, Zr, Hf, Y, and Th), including REE (Rare Earth Element, Figure 4c) are positively correlated with  $\text{SiO}_2$ . All are characterized by a linear positive correlation up to  $\text{SiO}_2 \approx 63\%$  and an almost vertical steepening of the trend for the three most evolved samples. The sharp increase in evolved compositions is most pronounced for the more incompatible elements such as Rb, Nb, Zr, Hf, Th, and Ta, still evident for light REE (La and Ce), but less pronounced for mildly incompatible elements, for example, Y and heavy REE (Yb).

Multi-element plots of incompatible trace elements for selected more mafic (Figure 5a) and more evolved samples (Figure 5c) have a humped pattern, with a maximum at Th-U-Ta-Nb and a negative K anomaly. Evolved samples also show moderate Sr, P, and Ti negative anomalies. The REE patterns of mafic samples (Figure 5b) show a fractionated trend (e.g.,  $\text{La}_N/\text{Yb}_N \sim 30$ –45) without a negative Eu anomaly, whereas most evolved samples (Figure 5d) show a small negative Eu anomaly and are characterized by quite high LREE to MREE ratios (e.g.,  $\text{La}_N/\text{Yb}_N \sim 40$ –55) in contrast with a flat trend for the heavy REE ( $\text{Gd}_N/\text{Yb}_N < 2.5$  for samples with  $\text{SiO}_2 > 60\%$ ).

### 4.3. Radiogenic Isotopes

Radiogenic isotope systematics for more mafic samples display relatively low  $^{87}\text{Sr}/^{86}\text{Sr}$  (<0.7038), moderately high  $^{143}\text{Nd}/^{144}\text{Nd}$  (>0.51284) and quite high  $^{206}\text{Pb}/^{204}\text{Pb}$  (c. 19.0–19.2), although typical HIMU (high  $\mu = ^{238}\text{U}/^{204}\text{Pb}$ ) values are not reached. Overall, most of the samples in the MMVG, both coastal lavas and those from the Mount Melbourne and Malta Plateau Volcanic fields, lie on the Sr-Nd isotopic mantle array, trending from Depleted MORB Mantle (DMM) to BSE (Bulk Silicate Earth) and clustering into the so-called Focal Zone

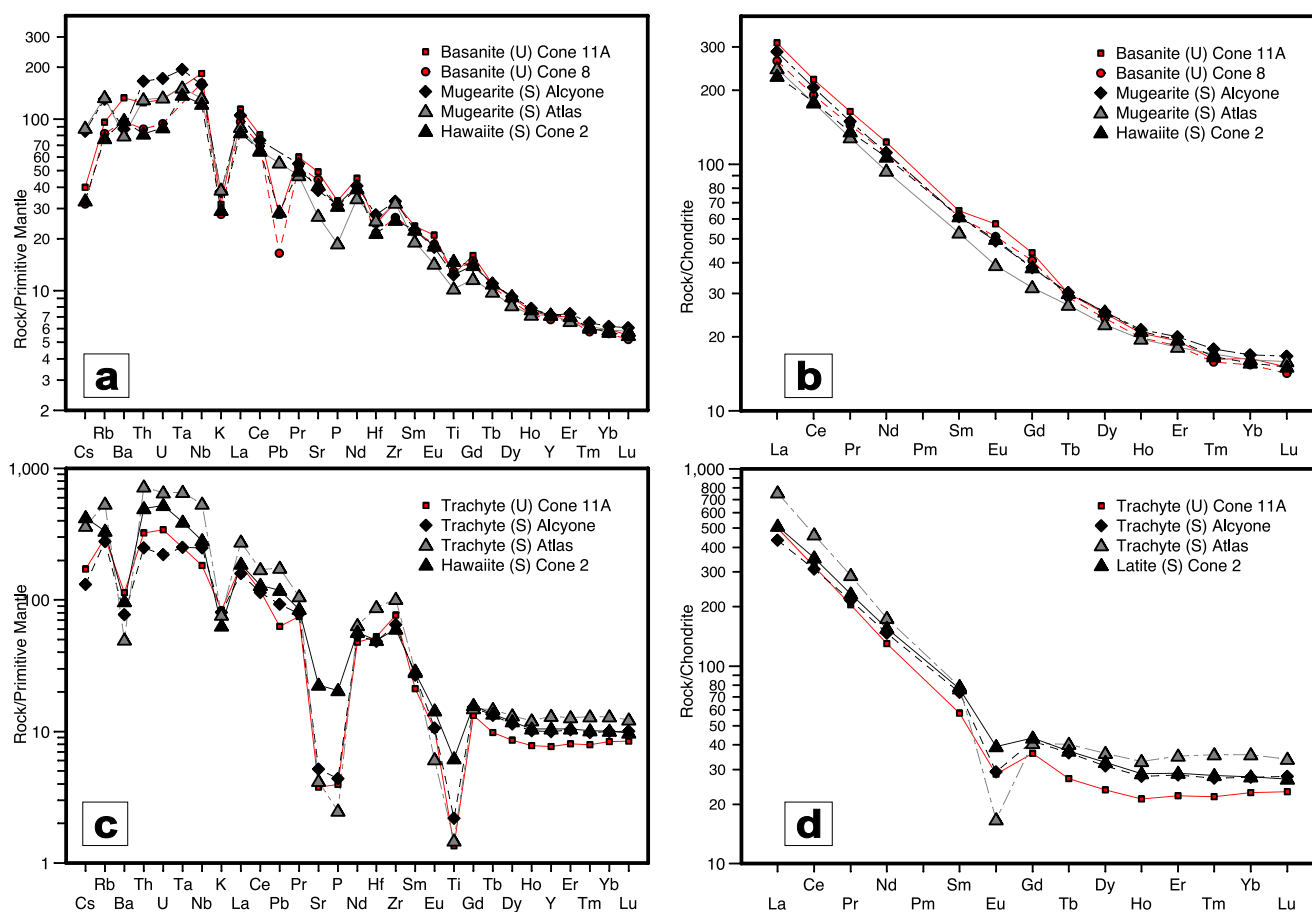


**Figure 5.** Multielemental plots for Incompatible Trace Elements (a and c) and REE (b and d) for selected samples of The Pleiades Volcanic Field. Normalizing values after McDonough and Sun (1995).

(FOZO, Figure 6a) On the contrary, our samples from The Pleiades exhibit quite large variations especially when compared with literature samples, mostly falling outside of FOZO. They depict an almost flat trend deviating from the mantle array and reaching  $^{87}\text{Sr}/^{86}\text{Sr}$  as high as 0.7052 coupled with negligible  $^{143}\text{Nd}/^{144}\text{Nd}$  variations (down to 0.51278). Lead isotope ratios (Figure 6) for our samples, on the contrary, are characterized by very small variations, clustering between EMII, FOZO and MORB, and above the NHRL (Northern Hemisphere Reference Line, Hart, 1984) both in the  $^{207}\text{Pb}/^{204}\text{Pb}$  versus  $^{206}\text{Pb}/^{204}\text{Pb}$  and  $^{208}\text{Pb}/^{204}\text{Pb}$  versus  $^{206}\text{Pb}/^{204}\text{Pb}$  diagrams. Some of the published samples from The Pleiades as well as other coastal lavas vary more widely and depict a trend crossing the NHRL.

#### 4.4. $^{40}\text{Ar}$ - $^{39}\text{Ar}$ Results

The Pleiades have long been considered as a possibly active (dormant) volcano (Geyer, 2021) based on published poorly constrained (high error) K-Ar (Armstrong, 1978) and  $^{40}\text{Ar}$ - $^{39}\text{Ar}$  (Esser & Kyle, 2002) ages, whose error bars include 0 ka ages. With the aim of constraining the youngest eruption age at The Pleiades, we selected for dating (a) a sample of comenditic trachyte pumice (JS3) from Mt. Atlas, occurring as lapilli and blocks mantling several of The Pleiades scoria cones, and (b) a sample from the Mt. Taygete lava dome (JS16), with the youngest published age, was also directly overlain by comenditic pumice.

Alkali-feldspar separates from both samples gave concordant age spectra, which exhibit some overlaps within uncertainties (Figure 7a). Weighted means, however, do not overlap within internal uncertainties, yielding ages of  $33.3 \pm 3.2$  ka ( $\pm 2\sigma$ ) and  $24.7 \pm 2.6$  ka ( $\pm 2\sigma$ ) for samples JS3 and JS16, respectively. In an  $^{36}\text{Ar}/^{40}\text{Ar}$  versus  $^{39}\text{Ar}/^{40}\text{Ar}$  isochron diagram (Figure 7b), sample JS16 (excluding the two initial heating steps yielding negative  $^{40}\text{Ar}^*/^{39}\text{Ar}$  ratios, data repository 4) an intercept age of  $24.8 \pm 3.0$  ka is indicated, in close agreement with the

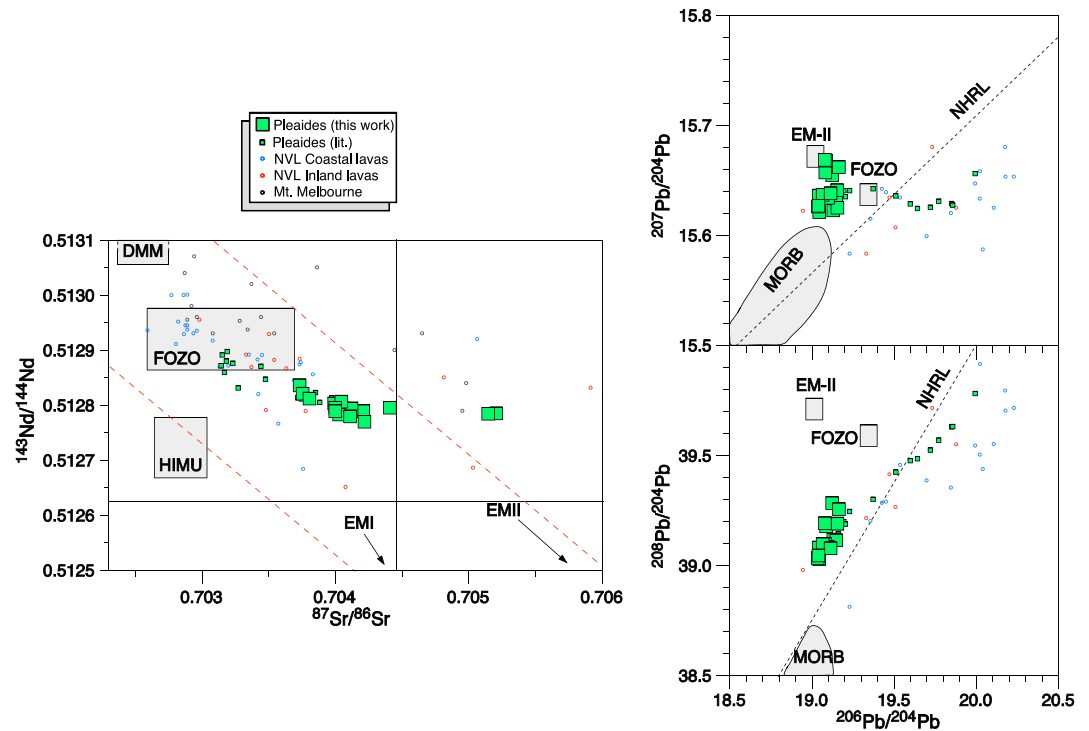


**Figure 6.** Radiogenic isotope diagrams ( $^{143}\text{Nd}/^{144}\text{Nd}$  vs.  $^{87}\text{Sr}/^{86}\text{Sr}$ ,  $^{207}\text{Pb}/^{204}\text{Pb}$  and  $^{208}\text{Pb}/^{204}\text{Pb}$  vs.  $^{206}\text{Pb}/^{204}\text{Pb}$ ) for samples of the Pleiades Volcanic Field. Other volcanic rocks from the NVL region are plotted for comparative purposes. Main mantle End Members have also been reported (Agostini et al., 2021).

weighted-mean age from the same sample. In contrast, sample JS3 gave a significantly younger isochron age of  $27.8 \pm 5.2$  ka, with an initial  $^{40}\text{Ar}/^{36}\text{Ar}$  ratio of  $307.6 \pm 7.2$  ( $\pm 2\sigma$ ), distinctly greater than that of modern atmospheric argon ( $^{40}\text{Ar}/^{36}\text{Ar}$  ratio of  $\sim 298.6$ ), which may be diagnostic of contamination by parentless  $^{40}\text{Ar}$  (excess argon) hosted in fluid or melt inclusions. The intercept ages from isochron plots of the two samples are indistinguishable within internal uncertainties, yielding a mean of  $25.6 \pm 2.5$  ka. In the light of the available data, we therefore consider the ages obtained from the isochron plots more reliable due to the likely occurrence of excess argon in sample JS3 and we infer that the two edifices investigated were constructed nearly synchronously at  $\sim 26$  ka.

Available geochronological data from the literature together with our new step-heating analyses, therefore, suggest that scattered volcanism occurred in a quite large time interval ( $\sim 0.85$  Ma). However, the youngest

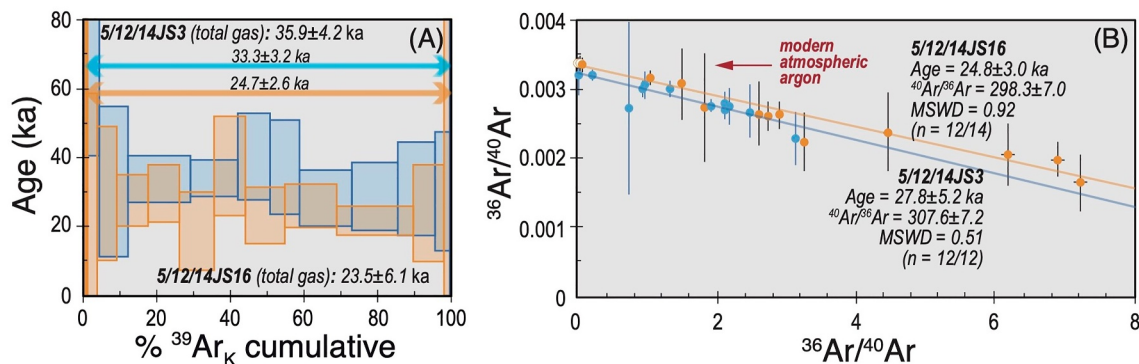


**Figure 7.** (a) Age spectra and (b) isochron plots (3-isotope correlation diagram,  $^{36}\text{Ar}/^{40}\text{Ar}$  vs.  $^{39}\text{Ar}/^{40}\text{Ar}$ ) for  $^{40}\text{Ar}$ - $^{39}\text{Ar}$  step-heating experiments of two selected samples of The Pleiades.

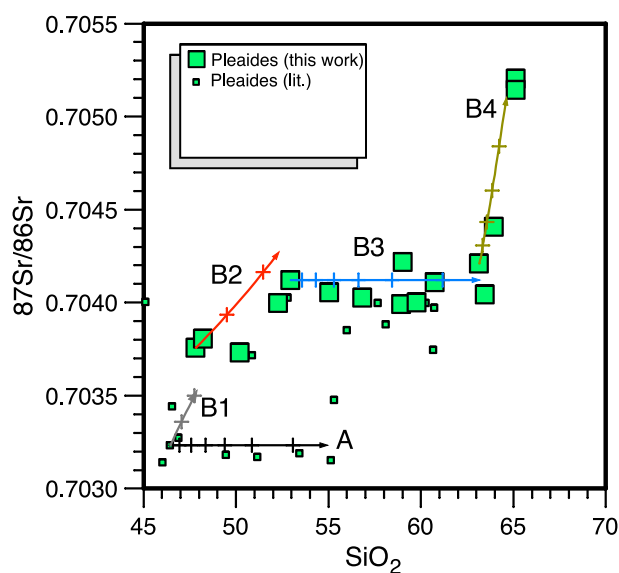


**Figure 8.**  $\text{SiO}_2$  versus  $^{87}\text{Sr}/^{86}\text{Sr}$  diagram for The Pleiades samples. Trends of FC (A) and AFC (B1–B4) modeling are also shown. For explanation, see the text.

climax of activity occurred at  $\sim 26$  ka, building in a relatively short time span ( $3 \pm 6$  ka) the most prominent edifices of The Pleiades (Mount Atlas and Mount Pleiones and associated subsidiary centers).

## 5. Discussion

### 5.1. Magma Genesis and Evolution

Overall, the least evolved samples of The Pleiades are Na-alkali basalts with trace element and isotopic signatures much like other basalts from NVL, therefore sharing with them a common origin linked to the Cenozoic evolution of the West Antarctic Rift System (WARS) (Durkin et al., 2023; Kim et al., 2019; Nardini et al., 2009; Panter et al., 2018; S. Rocchi & Smellie, 2021; S. Rocchi et al., 2002). According to S. Rocchi et al. (2005) and S. Rocchi and Smellie (2021), the mantle source was previously metasomatized during the Cretaceous amagmatic orthogonal rifting stage of the WARS. Since the Middle Miocene, magmas rose through N-S oriented faults that were mostly active on the western margin of the Ross Sea and are conjugate to a prominent NW-SE trans-lithospheric fault system (Nardini et al., 2009; Salvini et al., 1997; Storti et al., 2007).

At The Pleiades, a complete differentiation trend is observed, which is unique in NVL. Indeed, MMVG monogenetic scoria cones usually have basaltic compositions, and even in large volcanic edifices, intermediate compositions are scarce (i.e., Daly compositional gap, S. Rocchi & Smellie, 2021). Most of the volcanic products of The Pleiades are mildly Na-alkaline, slightly silica-undersaturated to saturated, and define a continuous differentiation trend, similar to other sodic, moderately alkaline lineages. Several samples from previous studies are richer in Na and silica-undersaturated, and do not define any clear lineage (Figure 3). Variations of major and trace elements against  $\text{SiO}_2$  (Figure 4) depict a continuous evolutionary trend at The Pleiades, and the significant co-variation of Sr isotope ratios with a modest decline in  $^{143}\text{Nd}/^{144}\text{Nd}$  (Figure 6) is indicative of open-system processes.

### 5.2. FC and AFC at The Pleiades

At The Pleiades, two distinct evolutionary trends are observed when radiogenic isotope variations are considered in detail (Figure 8). Path A shows low and constant Sr isotopic ratios ( $^{87}\text{Sr}/^{86}\text{Sr} \sim 0.7032$ ), irrespective of the degree of differentiation, consistent with closed-system evolutionary processes. Notably, this trend is only depicted by undersaturated samples with  $\text{SiO}_2$  variation restricted to the range 46–55 wt%. Path B, on the contrary, has a positive step-like correlation,  $^{87}\text{Sr}/^{86}\text{Sr}$  varying from 0.7032 to 0.7052 as  $\text{SiO}_2$  increases. Evolved samples from this trend have isotopic compositions shifted toward the average composition of NVL basement rocks (Di Vincenzo et al., 2014; Henjes-Kunst & Schüssler, 2003; S. Rocchi et al., 1998), suggesting that open-system evolution was operating with assimilation of crustal material.

In more detail, in path B we observe the occurrence of 3 jumps in  $^{87}\text{Sr}/^{86}\text{Sr}$  as well as a significant section of the path ( $\text{SiO}_2 = 52\text{--}63$  wt%) characterized by almost constant Sr isotopes ratios. Therefore, we define 4 evolutionary steps: from basanite to hawaiite (labeled B1 in Figure 8), then to mugearite (B2), to trachyte (B3) and finally to comenditic trachyte (B4). We modeled these steps as the FC-AFC process using the XLFRAC code for major elements (Stormer & Nicholls, 1978) and the equations of DePaolo (1981) for trace elements. Results are summarized in Table 1 and full calculations are available in data repository 5. Mineral chemistry data are from Supplementary Data of Kim et al. (2019).

Trend A is best modeled using a simple FC process, with a significant removal (66 wt%) of a gabbroic assemblage (Table 1). In trend B, Step B3 is again simple FC, whereas Steps B1, B2, and B4, despite quite limited  $\text{SiO}_2$  shifts, involve significant Sr isotope variations (Figure 8) much larger than those reported by Kim et al. (2019). These steps have therefore been modeled as open-system processes, using fractional crystallization coupled with assimilation of a crustal contaminant. We modeled the process differently from Kim et al. (2019), who calculated fractional crystallization for major elements separately from mixing calculations for radiogenic isotopes and used lower crustal material as contaminants, while we prefer upper crustal materials owing to the likely occurrence of

**Table 1**  
FC and AFC Model Results (Full Calculations Available in Data Repository 5)

Pleides complex FC and AFC modeling					
	Path A	Path B			
		Step 1	Step 2	Step 3	Step 4
From	K16012424	K16012424	JS10	JS4	JS15
	Alk Bas	Alk Bas	Hawaiite	Mugearite	Trachyte
To	K16012713-1	JS10	JS4	JS15	JS13 Com.
	Teph. Phonolite	Hawaiite	Mugearite	Trachyte	Trachyte
<b>Fractionating Phases</b>					
Olivine	10.6	3.9	5.8	3.4	3.3
Clinopyroxene	23.7	13.4	7.6	11.7	3.3
Plagioclase	22.0	3.9	7.2	41.2	3.0
Alk Feldspar					38.3
Ti-Magnetite	8.1	0.96	5.1	8.2	
Apatite	1.2		0.80	1.00	
<b>Fractionated Mass</b>	<b>65.7</b>	<b>22.1</b>	<b>26.6</b>	<b>65.5</b>	<b>47.9</b>
<b>Assimilated Mass</b>	–	<b>4.8</b>	<b>7.5</b>	–	<b>1.3</b>
<i>SSR</i>	<i>0.18</i>	<i>0.21</i>	<i>0.02</i>	<i>0.40</i>	<i>0.88</i>
<b>r (Assimilated Mass/Fractionated Mass Ratio)</b>	–	<b>0.22</b>	<b>0.28</b>	–	<b>0.027</b>
Pleides volume estimate (path B)					
Step	B4	B3	B2	B1	Start
	JS13 Com.	JS15	JS4	JS10	K16012424
	Trachyte	Trachyte	Mugearite	Hawaiite	Alk Bas
Vol ratio ( $V_F = 1$ )	1.00	1.92	5.56	7.58	9.73
Vol. est. ( $\text{km}^3$ ) ( $V_F = 7 \text{ km}^3$ )	7.00	13.44	38.94	53.06	68.11
Pleides versus Mt. Melbourne and Mt. Erebus					
Volcano name	Input data		Model calculation		
	Melbourne	Erebus	Pleides M <sup>a</sup>	Pleides E <sup>a</sup>	
Surface ( $\text{km}^2$ )	750.0	1,250.0			
Av. Radius (km)	15.5	19.9			
Height (km)	2.732	3.794			
Volume ( $\text{km}^3$ )	683.0	1,580.8			
Av. Radius/Height	5.7	5.3	5.7	5.3	
Volume ( $\text{km}^3$ )			68.1	68.1	
Av. Radius (km)			7.2	7.0	
Surface ( $\text{km}^2$ )			161.3	153.6	
Height (km)			1.267	1.330	

*Note.* In bold, amounts of fractionated mass, assimilated mass and their ratios, SSR (sum of square residuals) in italics. <sup>a</sup>Pleides M and Pleides E are the estimates of the dimensions of a Strato-Volcano having the same volumes of Pleiades with an aspect ratio of Mt Melbourne and Mt Erebus respectively

magma ponding at a relatively shallow crustal level. To model the path B, the composition of the crustal contaminant was chosen on the basis of the available geological mapping (Capponi et al., 2012). The basement rocks cropping out in the area of The Pleiades, in the north-west at Symes Nunatak and to the west and south-west at Eureka Spurs and Lawrence Peaks, are metasedimentary rocks of the Leap Year Group and Mariner Group of Bowers Terrane. We then selected an average of psammites from the Bowers Terrane (Henjes-Kunst & Schüssler, 2003) as the best representative of country rocks hosting the plumbing system of The Pleiades.

Fractionating phases were selected on the basis of petrographic observations. In more detail, according to XLFRAC mass balance, the B1 step (basanite to hawaiite) is best described by the removal of 22 wt% of a melagabbroic, cpx-dominated assemblage, with a rather high  $r$  (ratio between assimilated and fractionated material) of 0.22. The B2 step is characterized by  $\approx 27$  wt% removal of a gabbroic assemblage, and a high  $r$  of 0.28. The B3 step, covering the mugearite-trachyte evolution path with a 10 wt% SiO<sub>2</sub> increase, given the negligible Sr isotope variation, was modeled with a closed-system FC process. Here, a significant mass removal of 65 wt% of a plagioclase-dominated assemblage ( $\sim 63$  wt% of fractionating assemblage), along with a lesser amount of cpx ( $< 18$  wt%), Ti-magnetite ( $> 8\%$ ) and minor amounts of olivine ( $\sim 5\%$ ) and apatite ( $\sim 1.5$  wt%). Finally, the last step B4 is characterized by limited variations in all of the major elements, even if a significant mass removal of nearly 48 wt% is necessary to cover the trachyte to comenditic trachyte step. The fractionation assemblage is very different from the other steps, with alkali feldspar representing  $\sim 80\%$  of removed mass. The ratio of crustal assimilation is actually very low, with  $r \sim 0.027$ . Despite the low  $r$ , the large feldspar removal drives Sr concentrations to very low values, so that even a limited addition of contaminant results in a significant increment of the <sup>87</sup>Sr/<sup>86</sup>Sr ratio.

The robustness of this model was also tested with some other major and trace elements as well as trace element ratios. Full results are reported in data repository 5; in Figure 9 CaO, Rb as well as Sr/Y, Rb/Sr, Ba/Zr, and Zr/Y ratios are plotted against SiO<sub>2</sub>. We note that a simple AFC model has some limitations. For example, partition coefficients of trace elements may not be constant during evolution owing to variability of fractionating assemblage and chemical composition of minerals as well as possible fractionation of accessory phases are not considered here. In addition, no heat or energy budget is considered in determining the ratio between fractionated and assimilated material;  $r$  is also considered constant during each of the selected steps and for all the elements. Hence, it is modeled hypothesizing a bulk and linear assimilation of the host rock rather than considering differential diffusivity of some elements/isotopes, such as radiogenic Sr. Our model is therefore to be considered as semi-quantitative; a more quantitative model taking into account all these factors is beyond the scope of this paper and would require a set of assumptions that would make it poorly constrained by collected evidence. Despite this caveat, the model describes the compositional variations depicted in Figure 9 fairly well, with the sole exception for the B3 step involving HFSE such as Y and Zr, likely due to a role of zircon in the fractionating assemblage. As a whole, the results of the modeling and those shown in Figure 9 strongly support the occurrence of a complex evolving magmatic system, mostly characterized by open-system evolution, as also pointed out on the basis of textural features by I. Rocchi et al. (2024). The dispersion of data on some diagrams additionally highlights the possible occurrence of different secondary evolutionary stages/paths.

### 5.3. Magma Volumes in Coastal and Inland Locations

The Pleiades are characterized by an open-system evolutionary lineage in which all compositional members are represented, a quite unusual feature among NVL volcanic complexes (cf. S. Rocchi & Smellie, 2021). Unique conditions for magma fractionation and assimilation are therefore implicated. A principal feature that distinguishes The Pleiades from most other NVL volcanic complexes is their inland position. Inland, the history of rifting has led to a crustal setting that is different from the coastal zone, where most NVL volcanoes are located, causing the magmas to behave differently during their ascent to the surface. Volcanism was especially voluminous (in excess of 10<sup>4</sup> km<sup>3</sup>) along the coast (Adare, Hallett, Daniell peninsulas and Coulman Island: Hamilton, 1972; Kyle, 1990b; McIntosh & Kyle, 1990; Smellie, Rocchi, & Armienti, 2011; Wörner & Viereck, 1989) much more than in inland locations (including The Pleiades). Along the coast, magma production was enhanced due to the sharp crustal/lithospheric thickness transition across the Ross Sea coast, that coincides with a high thermal contrast (Faccenna et al., 2008). Thus, the NVL coast represented the weakest locus, where strain effects were significant, resulting in focused extension and lithospheric necking (Bonini et al., 2007; Huerta & Harry, 2007; Krans, 2013; Panter et al., 2018). Melts rising into the coast-parallel necking zone generated multiple, coalescing, large, mainly mafic volcanic shields. In contrast, melts ascending further inland in the thicker crust led to the establishment of crustal magma chambers, where extended fractionation occurred coupled with assimilation of crustal materials (S. Rocchi & Smellie, 2021). This resulted in a few relatively small and scattered mafic–felsic stratovolcanoes, among which Mount Overlord is morphologically prominent, while Mount Rittmann, the Malta Plateau centers and The Pleiades complex are characterized by volcanic features barely emerging from the ice cover. It is noticeable that these inland edifices are also hosts to all of the peralkaline products (including trachytes and rhyolites) in northern Victoria Land (S. Rocchi & Smellie, 2021). In Marie Byrd

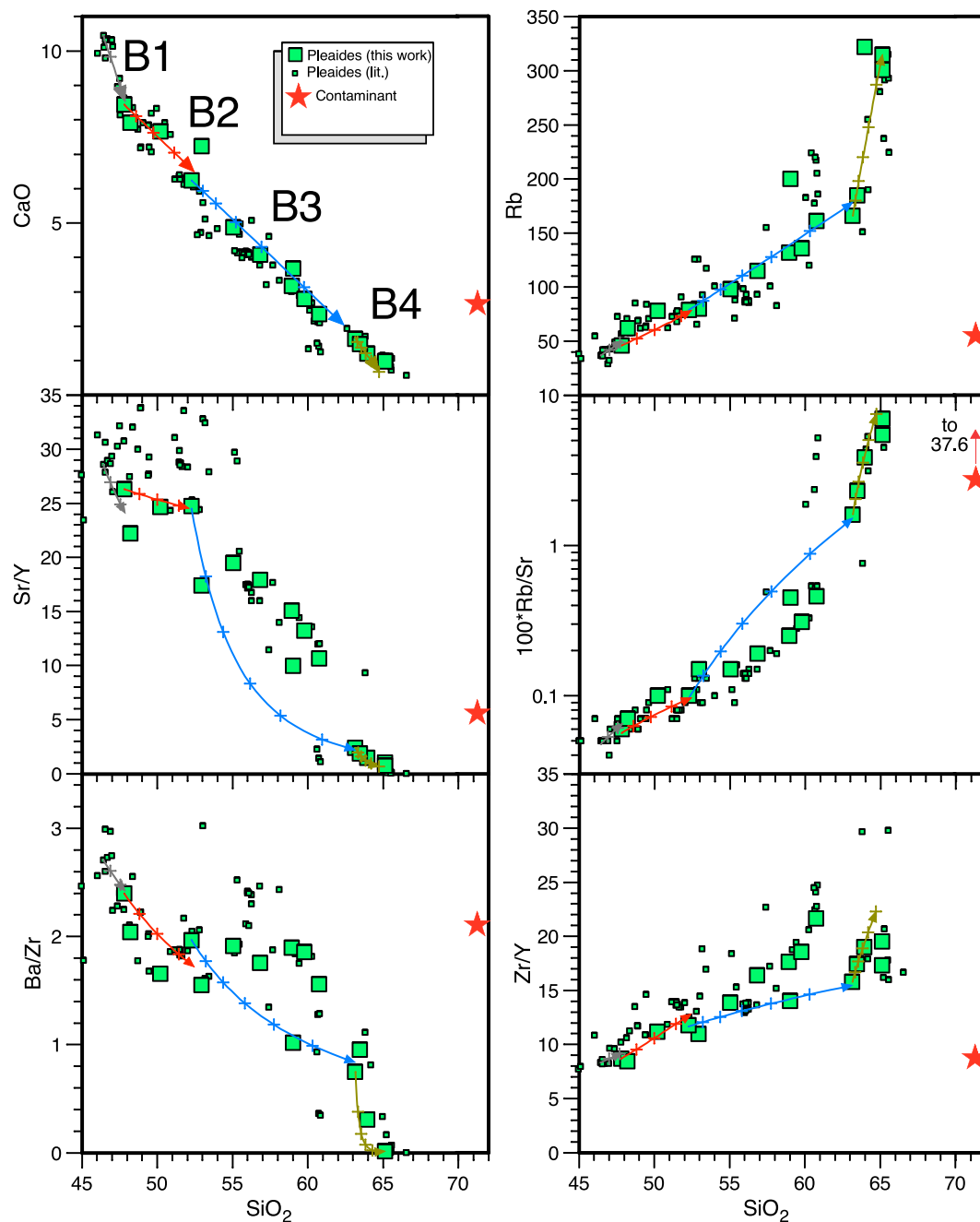


**Figure 9.** Trend of AFC (B1–B4) modeling in CaO, Sr/Y, Ba/Zr, Rb, Rb/Sr, and Zr/Y versus SiO<sub>2</sub> diagram for The Pleiades Volcanic Field. For explanation, see the text.

Land, peralkaline magmas are inferred to have been produced by fractional crystallization of basanite and removal of kaersutite at high pressure and plagioclase at low pressure (LeMasurier et al., 2011, 2018; Panter et al., 1997). By analogy, for NVL, we infer the occurrence of complex multi-level plumbing systems under the inland volcanoes resulting in the production of peralkaline magmas (S. Rocchi & Smellie, 2021).

At The Pleiades, a rough estimate of the erupted magma volume (Table 1) is about 21 km<sup>3</sup>, based on the area of 70 km<sup>2</sup> covered by The Pleiades and an average relief of ~300 m. Assuming that about one third of that volume (~7 km<sup>3</sup>) is represented by the most evolved magma composition (i.e., the comenditic trachytes), our fractionation models indicate a volume of primitive magmas ~10 times larger, that is, ~68 km<sup>3</sup> of total volume. This suggests the presence of a relatively large magma plumbing system within which most of the magma stalled. Had

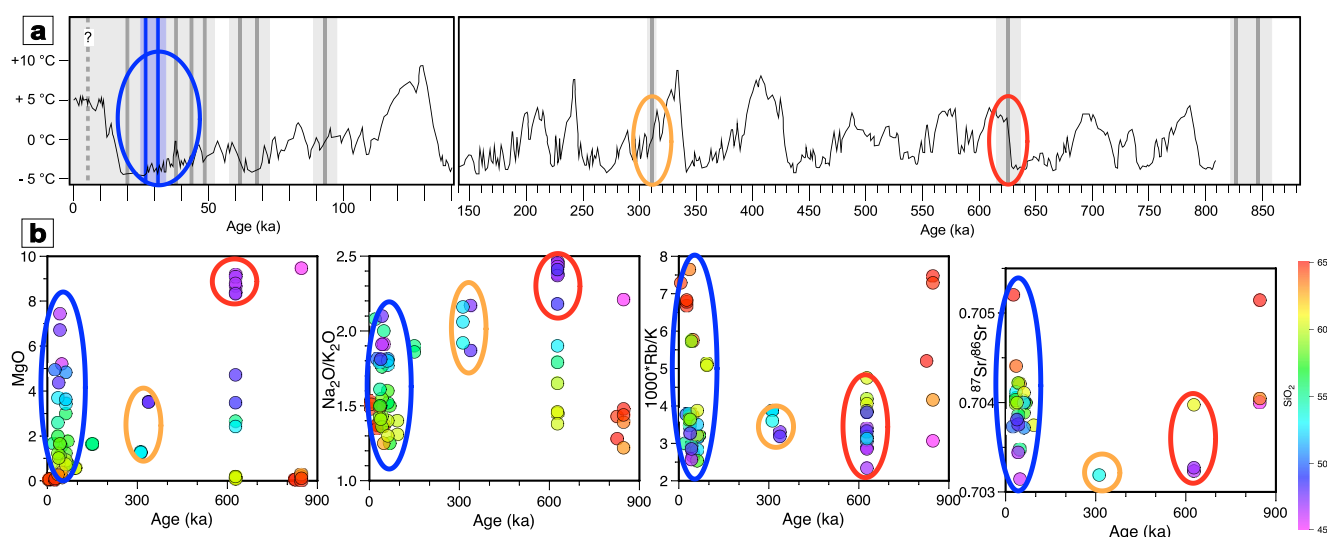


**Figure 10.** Age distribution and geochemical variation of The Pleiades Samples. (a) Timing of volcanic activity at The Pleiades (gray lines) compared with Antarctic Temperature Variation (redrawn from Jouzel et al. (2007)). (b) Ages of The Pleiades versus MgO, Na<sub>2</sub>O/K<sub>2</sub>O, Rb/K, and <sup>87</sup>Sr/<sup>86</sup>Sr diagrams, SiO<sub>2</sub> contents also shown. Both (a) and (b) highlight three major events of Pleiades. The oldest one (at about 830 ka) has not been highlighted because no T data are available. 630 ka event, red ellipses; 340–310 ka event, green ellipses, 50–25 Ka, blue ellipses.

all the magma erupted, it would have been capable of building a stratovolcano as high as ~1,300 m rather than the 20–30 partly coalesced monogenetic cones seen today (see Table 1 for further details).

#### 5.4. Paleoclimate Evolution and Magmatic Activity—A Role for Ice Cap in Magma Evolution

The occurrence at The Pleiades of a complete fractionation trend associated with prolonged stalling of magma in the plumbing system and significant crustal assimilation rate is unusual, almost unique among monogenetic (and/or polygenetic) alkaline volcanic fields globally in which bimodal compositions are common (e.g., Bonnefoi et al., 1995; Daly, 1925). In addition, The Pleiades Volcanic Field differs significantly from all of the other MMVG volcanoes located inland: (a) most of the latter comprise a volcanic field made up by multiple monogenetic cones (Northern Local Suite: Smellie & Rocchi, 2021) rather than polygenetic stratovolcanoes, (b) they are situated quite far from the coast (~130 km) and, as a consequence, (c) the basement on which the volcano was constructed is not located close to sea level, but has an elevation of c. 2,400 m asl. Thus, the differences in climatic conditions between The Pleiades and most other NVL volcanoes may be significant. In particular, the ice cover associated with The Pleiades is, and likely was in the past, thicker than at almost all other volcanoes in the region, which are located in coastal positions.

The Pleiades Volcanic Field erupted over >800 ka up to the present. During that period, numerous significant oscillations in temperature and, hence, ice thickness have been documented (e.g., EPICA ice-cores; Jouzel et al., 2007). In this context, the glacial load over The Pleiades was, correspondingly, affected by significant variations in thickness. Thus, it is important to evaluate the potential role of the glacial load in affecting the residence time of magma pulses in shallow plumbing systems and the eruption tempo. The published ages (Esser & Kyle, 2002), together with our new data, indicate that at least four major periods of eruptive activity have occurred: the oldest episode occurred at ~830 ka, a second one at ~630 ka, a third at 310–340 ka, and a final episode characterized by at least 10 eruptions between 70 ka and present, with a climax around 50–25 ka. We have compared the compositional features and the ages (where available) of the main eruptive events with climate variability during this time span, restricting our discussion to the three younger eruptive episodes at 630, 310–340 and <70 ka, owing the upper limit of 800 ka for the best documented local variations of temperature (Figure 10). When age data and chemical parameters are considered together, it is possible to notice that the 630 ka event differs when compared with the youngest phase in that it includes the most mafic compositions (lowest SiO<sub>2</sub>, highest MgO and Na<sub>2</sub>O/K<sub>2</sub>O contents). They also exhibit relatively low Rb/K ratios, and Sr isotope ratios are low and exhibit little variation, implying limited or no crustal assimilation. By contrast, the highest values of <sup>87</sup>Sr/<sup>86</sup>Sr as well as Rb/K ratios occur in samples associated with the youngest phase of activity, in which high-MgO and high-

Na<sub>2</sub>O/K<sub>2</sub>O samples are missing. Overall, we suggest that samples from the 630 ka event (and possibly those from 300 ka event, which lack sufficient data to disambiguate) tend to be more mafic and less affected by open system evolution, whereas those from the youngest phase, as well as those from oldest 830 ka event, exhibit more complex and open-system evolutionary patterns associated with significant crustal assimilation. Moreover, samples from the climax of activity at 25–50 ka display both high compositional variabilities, as evidenced by the wide MgO and SiO<sub>2</sub> ranges, the highest degree of fractionation as well as the largest amount of crustal contamination marked by the highest Rb/K ratios and <sup>87</sup>Sr/<sup>86</sup>Sr of the whole data set. When we compare these compositional characteristics with the record of Antarctic temperatures (Jouzel et al., 2007) (Figure 10a), we notice that the 630 ka event, despite the uncertainties, likely developed in a relatively warm period, as did the 300 ka event. The youngest phase, on the contrary, had its climax toward the end of the last glacial period, when the ice cover reached its maximum thickness. These observations suggest that variations in the thickness of the ice cover may have played a role in modulating chemical fractionation in The Pleiades plumbing system since (a) warm conditions, corresponding to a reduced ice thickness, favored the emplacement of poorly evolved (including primitive) products, which lack significant fractional crystallization (i.e., path A in Figure 8); (b) by contrast, the erupted magmas that depict more complex evolutionary paths (i.e., paths B1–B4 in Figures 8 and 9), indicate a more extended compositional evolution and strong crustal assimilation linked to a longer residence time in the crust that may have been imposed by the ice loading during the colder conditions that prevailed during the last 70 ka and particularly at 50–25 ka. It is notable that erupted compositions associated with the youngest events, which were responsible for building the two most prominent edifices, exhibit the highest differentiation and crustal assimilation rates and erupted close to the end of the last glacial period, when the ice cover should have been much thicker.

## 6. Conclusions

The Pleiades is a peculiar volcanic field in Antarctica. It consists mainly of a series of often-overlapping scoria cones and thus resembles the numerous small monogenetic centers that characterize the Northern Local Suite in northern Victoria Land. On the other hand, The Pleiades volcanic field is located in an inland position relative to most of the other volcanic complexes in NVL and we can infer that it is part of a larger polygenetic volcanic field, now mostly obscured by ice and snow, with a large plumbing system below. The erupted magmas are characterized by a continuous differentiation trend unique to the region, and the magma compositional features demonstrate high rates of assimilation of crustal material in most of the erupted products. These reveal the occurrence of an unexpectedly large complex plumbing system and confirm a polygenetic origin for The Pleiades Volcanic Field. We infer that these unique features may be a consequence of their special location, situated inland and associated with an ice cover that, when it was thicker than present, helped to temporarily suppress eruptions, thus imposing a long magma residence time in the subsurface that favored significant fractionation and unusually high rates of crustal assimilation.

## Data Availability Statement

Data supporting this paper are available in the following Data Repository: Agostini et al. (2024).

## References

- Agostini, S., Di Giuseppe, P., Manetti, P., Doglioni, C., & Conticelli, S. (2021). A heterogeneous subcontinental mantle under the African-Arabian Plate boundary revealed by boron and radiogenic isotopes. *Scientific Reports*, *11*(1), 11230. <https://doi.org/10.1038/s41598-021-90275-7>
- Agostini, S., Leone, N., Smellie, J. L., & Rocchi, S. (2024). Geochemical, isotopic, geochronological data and assimilation plus fractional crystallization model of The Pleiades Volcanic Field (Northern Victoria Land, Antarctica) [Dataset]. *GFZ Data Services*. <https://doi.org/10.5880/idgeo.2024.001>
- Armstrong, R. L. (1978). K-Ar dating: Late Cenozoic McMurdo Volcanic Group and dry valley glacial history, Victoria Land, Antarctica. *New Zealand Journal of Geology and Geophysics*, *21*(6), 685–698. <https://doi.org/10.1080/00288306.1978.10425199>
- Bonini, M., Corti, G., Ventisette, C. D., Manetti, P., Mulugeta, G., & Sokoutis, D. (2007). Modelling the lithospheric rheology control on the Cretaceous rifting in West Antarctica. *Terra Nova*, *19*(5), 360–366. <https://doi.org/10.1111/j.1365-3121.2007.00760.x>
- Bonnefoi, C. C., Provost, A., & Albarède, F. (1995). The “Daly gap” as a magmatic catastrophe. *Nature*, *378*(6554), 270–272. <https://doi.org/10.1038/378270a0>
- Capponi, G., Meccheri, M., Pertusati, P. C., Carosi, R., Crispini, L., Musumeci, G., et al. (2012). Antarctic geological 1:250,000 map series. Freyberg Mountains Quadrangle (Victoria Land). In P. C. Pertusati & F. Tessensohn (coordinators), *GIGAMAP*.
- Daly, R. A. (1925). The geology of ascension Island. *Proceedings of the American Academy of Arts and Sciences*, *60*, 1–80. <https://doi.org/10.2307/25130043>
- DePaolo, D. J. (1981). Trace element and isotopic effects of combined wallrock assimilation and fractional crystallisation. *Earth and Planetary Science Letters*, *53*(2), 189–202. [https://doi.org/10.1016/0012-821x\(81\)90153-9](https://doi.org/10.1016/0012-821x(81)90153-9)

## Acknowledgments

Thanks are due to G. Di Vincenzo (IGG-CNR) for <sup>40</sup>Ar-<sup>39</sup>Ar analyses. E. Regattieri (IGG-CNR) is acknowledged for stimulating discussions on paleoclimate reconstruction. The authors are also grateful to Kurt Panter and Kelly Russell for their supportive and detailed reviews, which helped to improve the paper. This work has been financially supported by the National Research Antarctic Programme of Italy (PNRA2013/AZ2.07 and PNRA18\_00037-Magic). Open access publishing facilitated by Università degli Studi di Pisa, as part of the Wiley - CRUI-CARE agreement.

- Di Roberto, A., Colizza, E., Del Carlo, P., Petrelli, M., Finocchiaro, F., & Kuhn, G. (2019). First marine cryptotephra in Antarctica found in sediments of the western Ross Sea correlates with glacial tephra and climate records. *Scientific Reports*, *9*(1), 10628. <https://doi.org/10.1038/s41598-019-47188-3>
- Di Vincenzo, G., Bracciali, L., Del Carlo, P., Panter, K., & Rocchi, S. (2010).  $^{40}\text{Ar}$ - $^{39}\text{Ar}$  dating of volcanogenic products from the AND-2A core (ANDRILL Southern McMurdo sound project, Antarctica): Correlations with the Erebus Volcanic Province and implications for the age model of the core. *Bulletin of Volcanology*, *72*(4), 487–505. <https://doi.org/10.1007/s00445-009-0337-z>
- Di Vincenzo, G., Grande, A., & Rossetti, F. (2014). Paleozoic siliciclastic rocks from northern Victoria Land (Antarctica): Provenance, timing of deformation, and implications for the Antarctica-Australia connection. *Geological Society of America Bulletin*, *126*(11–12), 1416–1438. <https://doi.org/10.1130/B31034.1>
- Durkin, K., Day, J. M. D., Panter, K. S., Xu, J.-F., & Castillo, P. R. (2023). Petrogenesis of alkaline magmas across a continent to ocean transect, northern Ross Sea, Antarctica. *Chemical Geology*, *641*, 121780. <https://doi.org/10.1016/j.chemgeo.2023.121780>
- Edwards, B. R., Russell, J. K., & Anderson, R. G. (2002). Subglacial, phonolitic volcanism at Hoodoo Mountain volcano, northern Canadian Cordillera. *Bulletin of Volcanology*, *64*(3–4), 254–272. <https://doi.org/10.1007/s00445-002-0202-9>
- Esser, R., & Kyle, P. (2002).  $^{40}\text{Ar}$ - $^{39}\text{Ar}$  chronology of the McMurdo Volcanic Group at the Pleiades, northern Victoria Land. *Antarctica*, *35*, 415–418.
- Faccenna, C., Rossetti, F., Becker, T. W., Danesi, S., & Morelli, A. (2008). Recent extension driven by mantle upwelling beneath the Admiralty Mountains (East Antarctica). *Tectonics*, *27*(4), TC4015. <https://doi.org/10.1029/2007TC002197>
- Geyer, A. (2021). Chapter 1.4 Antarctic volcanism: Active volcanism overview. In J. L. Smellie, K. S. Panter, & A. Geyer (Eds.), *Volcanism in Antarctica: 200 million years of subduction, rifting and continental break-up* (pp. 55–72). Geological Society.
- Geyer, A., & Bindeman, I. (2011). Glacial influence on caldera-forming eruptions. *Journal of Volcanology and Geothermal Research*, *202*(1–2), 127–142. <https://doi.org/10.1016/j.jvolgeores.2011.02.001>
- Glazner, A. F., Manley, C. R., Marron, J. S., & Rojstaczer, S. (1999). Fire or ice: Anticorrelation of volcanism and glaciation in California over the past 800,000 years. *Geophysical Research Letters*, *26*(12), 1759–1762. <https://doi.org/10.1029/1999gl900333>
- Grove, E. W. (1974). Deglaciation—A possible triggering mechanism for recent volcanism. In *Proceedings symposium of Andean and Antarctic volcanology* (pp. 88–97).
- Hamilton, W. (1972). The Hallet Volcanic Province, Antarctica (p. 62).
- Hart, S. R. (1984). A large-scale isotope anomaly in the Southern Hemisphere mantle. *Nature*, *309*(5971), 753–757. <https://doi.org/10.1038/309753a0>
- Henjes-Kunst, F., & Schüssler, U. (2003). Metasedimentary units of the Cambro-Ordovician Ross Orogen in northern Victoria Land and Oates Land: Implications for their provenance and geotectonic setting from geochemical and Nd-Sr isotope data. *Terra Antarctica*, *10*(3), 105–128.
- Huerta, A. D., & Harry, D. L. (2007). The transition from diffuse to focused extension: Modeled evolution of the West Antarctic Rift system. *Earth and Planetary Science Letters*, *255*(1–2), 133–147. <https://doi.org/10.1016/j.epsl.2006.12.011>
- Huybers, P., & Langmuir, C. (2009). Feedback between deglaciation, volcanism, and atmospheric CO<sub>2</sub>. *Earth and Planetary Science Letters*, *286*(3–4), 479–491. <https://doi.org/10.1016/j.epsl.2009.07.014>
- Jouzel, J., Masson-Delmotte, V., Cattani, O., Dreyfus, G., Falourd, S., Hoffmann, G., et al. (2007). Orbital and millennial Antarctic climate variability over the past 800,000 years. *Science*, *317*(5839), 793–796. <https://doi.org/10.1126/science.1141038>
- Jull, M., & McKenzie, D. (1996). The effect of deglaciation on mantle melting beneath Iceland. *Journal of Geophysical Research*, *101*(B10), 21815–21828. <https://doi.org/10.1029/96jb01308>
- Kim, J., Park, J.-W., Lee, M. J., Lee, J. I., & Kyle, P. R. (2019). Evolution of alkalic magma systems: Insight from coeval evolution of sodic and potassic fractionation lineages at the Pleiades volcanic complex, Antarctica. *Journal of Petrology*, *60*(1), 117–150. <https://doi.org/10.1093/ptrology/egy108/5230997>
- Krans, S. R. (2013). New mineral chemistry and oxygen isotopes from alkaline basalts in the Northwest Ross Sea, Antarctica: Insights on magma genesis across rifted continental and oceanic lithosphere. MSc Thesis (p. 91). Bowling Green State University.
- Kyle, P. R. (1982). Volcanic geology of The Pleiades, northern Victoria Land, Antarctica. In C. Craddock (Ed.), *In Antarctic Geosciences* (pp. 747–754). University of Wisconsin Press.
- Kyle, P. R. (1986). Mineral chemistry of late Cenozoic McMurdo volcanic group—Rocks from the Pleiades, northern Victoria Land. In *Geological investigations in northern Victoria Land—Antarctic Research series* (pp. 305–337).
- Kyle, P. R. (1990a). McMurdo Volcanic Group. Western Ross embayment. Introduction. In W. E. LeMasurier, & J. W. Thomson (Eds.), *Volcanoes of the Antarctic Plate & southern oceans* (pp. 19–25).
- Kyle, P. R. (1990b). Melbourne Volcanic Province. In W. E. LeMasurier, & J. W. Thomson (Eds.), *Volcanoes of the Antarctic Plate & southern oceans* (pp. 48–80).
- Kyle, P. R. (1990c). The Pleiades. In W. E. LeMasurier, & J. W. Thomson (Eds.), *Volcanoes of the Antarctic Plate & southern oceans* (pp. 60–64).
- Kyle, P. R., & Rankin, P. C. (1976). Rare earth element geochemistry of late Cenozoic alkaline lava of the McMurdo Volcanic Group, Antarctica. *Geochimica et Cosmochimica Acta*, *40*(12), 1497–1507. [https://doi.org/10.1016/0016-7037\(76\)90089-2](https://doi.org/10.1016/0016-7037(76)90089-2)
- Lee, M. J., Kyle, P. R., Iverson, N. A., Lee, J. I., & Han, Y. (2019). Rittmann volcano, Antarctica as the source of a widespread  $1252 \pm 2$  CE tephra layer in Antarctica ice. *Earth and Planetary Science Letters*, *521*, 169–176. <https://doi.org/10.1016/j.epsl.2019.06.002>
- LeMasurier, W., Choi, S. H., Kawachi, Y., Mukasa, S., & Rogers, N. (2018). Dual origins for pantellerites, and other puzzles, at Mount Takaha volcano, Marie Byrd Land, West Antarctica. *Lithos*, *296–299*, 142–162. <https://doi.org/10.1016/j.lithos.2017.10.014>
- LeMasurier, W. E., Hi Choi, S., Kawachi, Y., Mukasa, S. B., & Rogers, N. W. (2011). Evolution of pantellerite-trachyte-phonolite volcanoes by fractional crystallization of basanite magma in a continental rift setting, Marie Byrd Land, Antarctica. *Contributions to Mineralogy and Petrology*, *162*(6), 1165–1179. <https://doi.org/10.1007/s00410-011-0646-z>
- W. E. LeMasurier, & J. W. Thomson (Eds.) (1990). *Volcanoes of the Antarctic Plate and southern oceans* (p. 487). American Geophysical Union.
- MacLennan, J., Jull, M., McKenzie, D., Slater, L., & Grönvold, K. (2002). The link between volcanism and deglaciation in Iceland. *Geochemistry, Geophysics, Geosystems*, *3*(11), 1062–1125. <https://doi.org/10.1029/2001GC000282>
- McDonough, W. F., & Sun, S. S. (1995). The composition of the Earth. *Chemical Geology*, *120*(3–4), 223–253. [https://doi.org/10.1016/0009-2541\(94\)00140-4](https://doi.org/10.1016/0009-2541(94)00140-4)
- McIntosh, W. C., & Kyle, P. R. (1990). Hallett Volcanic Province. In W. E. LeMasurier, & J. W. Thomson (Eds.), *Volcanoes of the Antarctic Plate & southern oceans* (pp. 26–47).
- Middlemost, E. A. K. (1975). The Basalt clan. *Earth-Science Reviews*, *11*(4), 337–364. [https://doi.org/10.1016/0012-8252\(75\)90039-2](https://doi.org/10.1016/0012-8252(75)90039-2)
- Narcisi, B., Petit, J. R., & Langone, A. (2017). Last glacial tephra layers in the Talos Dome ice core (peripheral East Antarctic Plateau), with implications for chronostratigraphic correlations and regional volcanic history. *Quaternary Science Reviews*, *165*, 111–126. <https://doi.org/10.1016/j.quascirev.2017.04.025>

- Narcisi, B., Proposito, M., & Frezzotti, M. (2001). Ice record of a 13th century explosive volcanic eruption in northern Victoria Land, East Antarctica. *Antarctic Science*, 13(2), 174–181. <https://doi.org/10.1017/s0954102001000268>
- Nardini, I., Armienti, P., Rocchi, S., Dallai, L., & Harrison, D. (2009). Sr-Nd-Pb-He-O isotope and geochemical constraints on the genesis of Cenozoic magmas from the West Antarctic Rift. *Journal of Petrology*, 50(7), 1359–1375. <https://doi.org/10.1093/ptrology/egn082>
- Nathan, S., & Schulte, F. J. (1968). Geology and petrology of the Campbell—Aviator Divide, Northern Victoria Land, Antarctica. *New Zealand Journal of Geology and Geophysics*, 11(4), 940–975. <https://doi.org/10.1080/00288306.1968.10420762>
- Nyland, R. E., Panter, K. S., Rocchi, S., Di Vincenzo, G., Del Carlo, P., Tiepolo, M., et al. (2013). Volcanic activity and its link to glaciation cycles: Single-grain age and geochemistry of Early Miocene volcanic glass from ANDRILL AND-2A core, Antarctica. *Journal of Volcanology and Geothermal Research*, 250, 106–128. <https://doi.org/10.1016/j.jvolgeores.2012.11.008>
- Pagli, C., & Sigmundsson, F. (2008). Will present day glacier retreat increase volcanic activity? Stress induced by recent glacier retreat and its effect on magmatism at the Vatnajoˆkull ice cap, Iceland. *Geophysical Research Letters*, 35(9), L09304. <https://doi.org/10.1029/2008GL033510>
- Panter, K. S., Castillo, P., Krans, S., Deering, C., McIntosh, W., Valley, J. W., et al. (2018). Melt origin across a rifted continental margin: A case for subduction-related metasomatic agents in the lithospheric source of alkaline basalt, northwest Ross Sea, Antarctica. *Journal of Petrology*, 59(3), 517–558. <https://doi.org/10.1093/ptrology/egy036>
- Panter, K. S., Kyle, P. R., & Smellie, J. L. (1997). Petrogenesis of a phonolite-trachyte succession at Mount Sidley, Marie Byrd Land, Antarctica. *Journal of Petrology*, 38(9), 1225–1253. <https://doi.org/10.1093/ptrology/38.9.1225>
- Rawson, H., Pyle, D. M., Mather, T. A., Smith, V. C., Fontijn, K., Lachowycz, S. M., & Naranjo, J. A. (2016). The magmatic and eruptive response of arc volcanoes to deglaciation: Insights from southern Chile. *Geology*, 44(4), 251–254. <https://doi.org/10.1130/g37504.1>
- Riddolls, B. W., & Hancox, G. T. (1968). The geology of the upper Mariner Glacier region, North Victoria Land, Antarctica. *New Zealand Journal of Geology and Geophysics*, 11(4), 881–899. <https://doi.org/10.1080/00288306.1968.10420758>
- Rocchi, L., Tomassini, A., Masotta, M., Petrelli, M., Ágreda López, M., & Rocchi, S. (2024). Textures and chemistry of crystal cargo of The Pleiades volcanic field, Antarctica: Potential influence of ice load in modulating the plumbing system. *Journal of Petrology*, 65(4), egae027. <https://doi.org/10.1093/ptrology/egae027>
- Rocchi, S., Armienti, P., D'Orazio, M., Tonarini, S., Wijbrans, J., & Di Vincenzo, G. (2002). Cenozoic magmatism in the western Ross embayment: Role of mantle plume vs. plate dynamics in the development of the West Antarctic Rift system. *Journal of Geophysical Research*, 107(B9), 2195. <https://doi.org/10.1029/2001jb0000515>
- Rocchi, S., Di Vincenzo, G., & Armienti, P. (2005). No plume, no rift magmatism in the West Antarctic Rift. In G. R. Foulger, D. L. Anderson, J. H. Natland, & D. C. Presnall (Eds.), *Plates, plumes & paradigms* (Vol. 388, pp. 435–447). Geological Society of America Special Paper. <https://doi.org/10.1130/0-8137-2388-4.435>
- Rocchi, S., & Smellie, J. L. (2021). Chapter 5.1b northern Victoria land: Petrology. *Geological Society, London, Memoirs*, 55(1), 383–413. <https://doi.org/10.1144/m55-2019-19>
- Rocchi, S., Tonarini, S., Armienti, P., Innocenti, F., & Manetti, P. (1998). Geochemical and isotopic structure of the early Palaeozoic active margin of Gondwana in northern Victoria Land, Antarctica. *Tectonophysics*, 284(3–4), 261–281. [https://doi.org/10.1016/s0040-1951\(97\)00178-9](https://doi.org/10.1016/s0040-1951(97)00178-9)
- Salvini, F., Brancolini, G., Busetti, M., Storti, F., Mazzarini, F., & Coren, F. (1997). Cenozoic geodynamics of the Ross Sea region, Antarctica: Crustal extension, intraplate strike-slip faulting, and tectonic inheritance. *Journal of Geophysical Research*, 102(B11), 24669–24696. <https://doi.org/10.1029/97jb01643>
- Sigmundsson, F., Pinel, V., Lund, B., Albino, F., Pagli, C., Geirsson, H., & Sturkell, E. (2010). Climate effects on volcanism: Influence on magmatic systems of loading and unloading from ice mass variations, with examples from Iceland. *Philosophical Transactions of the Royal Society*, 368(1919), 2519–2534. <https://doi.org/10.1098/rsta.2010.0042>
- Sigvaldason, G. E., Annertz, K., & Nilsson, M. (1992). Effect of glacier loading/deloading on volcanism: Postglacial volcanic production rate of the Dyngjujöll area, central Iceland. *Bulletin of Volcanology*, 54(5), 385–392. <https://doi.org/10.1007/bf00312320>
- Slater, L., Jull, M., McKenzie, D., & Gronvˆld, K. (1998). Deglaciation effects on mantle melting under Iceland: Results from the northern volcanic zone. *Earth and Planetary Science Letters*, 164(1–2), 151–164. [https://doi.org/10.1016/s0012-821x\(98\)00200-3](https://doi.org/10.1016/s0012-821x(98)00200-3)
- Smellie, J., Rocchi, S., & Armienti, P. (2011). Late Miocene volcanic sequences in northern Victoria Land, Antarctica: Products of glaciovolcanic eruptions under different thermal regimes. *Bulletin of Volcanology*, 73, 1–25. <https://doi.org/10.1007/s00445-010-0399-y>
- Smellie, J. L., & Edwards, B. R. (2016). *Glaciovolcanism on Earth and Mars* (p. 483). Cambridge University Press.
- J. L. Smellie, K. S. Panter, & A. Geyer (Eds.) (2021a). *Volcanism in Antarctica: 200 million years of subduction, rifting and continental break-up* (Vol. 55, p. 803). Geological Society.
- Smellie, J. L., Panter, K. S., & Geyer, A. (2021b). Volcanism in Antarctica: 200 million years of subduction, rifting and continental break-up. *Geological Society, London, Memoirs*, 55(1), 1–6. <https://doi.org/10.1144/m55-2020-14>
- Smellie, J. L., & Rocchi, S. (2021). Chapter 5.1a northern Victoria Land: Volcanology. *Geological Society, London, Memoirs*, 55(1), 347–381. <https://doi.org/10.1144/m55-2018-60>
- Smellie, J. L., Rocchi, S., Gemelli, M., Di Vincenzo, G., & Armienti, P. (2011). A thin predominantly cold-based Late Miocene East Antarctic ice sheet inferred from glaciovolcanic sequences in northern Victoria Land, Antarctica. *Palaeogeography, Palaeoclimatology, Palaeoecology*, 307(1–4), 129–149. <https://doi.org/10.1016/j.palaeo.2011.05.008>
- Smellie, J. L., Rocchi, S., Johnson, J. S., Di Vincenzo, G., & Schaefer, J. M. (2018). A tuff cone erupted under frozen-bed ice (northern Victoria Land, Antarctica): Linking glaciovolcanic and cosmogenic nuclide data for ice sheet reconstructions. *Bulletin of Volcanology*, 80(1), 12. <https://doi.org/10.1007/s00445-017-1185-x>
- Smellie, J. L., Rocchi, S., Wilch, T. I., Gemelli, M., Di Vincenzo, G., McIntosh, W., et al. (2014). Glaciovolcanic evidence for a polythermal Neogene East Antarctic ice sheet. *Geology*, 42(1), 39–42. <https://doi.org/10.1130/g34787.1>
- Stormer, J. C., & Nicholls, J. (1978). XLFrac: A program for the interactive testing of magmatic differentiation. *Computers & Geosciences*, 4, 153–159.
- Storti, F., Salvini, F., Rossetti, F., & Phipps Morgan, J. (2007). Intraplate termination of transform faulting within the Antarctic continent. *Earth and Planetary Science Letters*, 260(1–2), 115–126. <https://doi.org/10.1016/j.epsl.2007.05.020>
- Wilson, A. M., & Russell, J. K. (2020). Glacial pumping of a magma-charged lithosphere: A model for glaciovolcanic causality in magmatic arcs. *Earth and Planetary Science Letters*, 548, 116500. <https://doi.org/10.1016/j.epsl.2020.116500>
- Wörner, G., & Viereck, L. (1989). The Mt. Melbourne volcanic field (Victoria Land, Antarctica). I. Field observations. *Geologisches Jahrbuch*, E38, 369–393.